NeuroImage 237 (2021) 118195

Contents lists available at ScienceDirect

NeuroImage

journal homepage: www.elsevier.com/locate/neuroimage

# Validating layer-specific VASO across species

Laurentius (Renzo) Huber[a,1,*], Benedikt A Poser[a], Amanda L Kaas[a], Elizabeth J Fear[b], Sebastian Dresbach[a], Jason Berwick[c], Rainer Goebel[a], Robert Turner[d,e], Aneurin J Kennerley[b,1,*]

[a] MBIC, Department of Cognitive Neuroscience, Faculty of Psychology and Neuroscience, Maastricht University, the Netherlands
[b] Hull-York-Medical-School (HYMS), University of York, York, United Kingdom
[c] Department of Psychology, University of Sheffield, Sheffield, United Kingdom
[d] Neurophysics Department Max Planck Institute for Human Cognitive and Brain Sciences, Leipzig, Germany
[e] Sir Peter Mansfield Imaging Centre, University of Nottingham, Nottingham, United Kingdom

ARTICLE INFO

*Keywords:*
fMRI
Laminar
Layer
Pre-clinical
Sub-millimetre
Somatosensory stimulation
Draining vein
Depth-dependent fMRI
Concurrent imaging
Optical imaging spectroscopy
Cerebral blood volume
MION
VASO.

ABSTRACT

Cerebral blood volume (CBV) has been shown to be a robust and important physiological parameter for quantitative interpretation of functional (f)MRI, capable of delivering highly localized mapping of neural activity. Indeed, with recent advances in ultra-high-field (≥7T) MRI hardware and associated sequence libraries, it has become possible to capture non-invasive CBV weighted fMRI signals across cortical layers. One of the most widely used approaches to achieve this (in humans) is through vascular-space-occupancy (VASO) fMRI. Unfortunately, the exact contrast mechanisms of layer-dependent VASO fMRI have not been validated for human fMRI and thus interpretation of such data is confounded. Here we validate the signal source of layer-dependent SS-SI VASO fMRI using multi-modal imaging in a rat model in response to neuronal activation (somatosensory cortex) and respiratory challenge (hypercapnia). In particular VASO derived CBV measures are directly compared to concurrent measures of total haemoglobin changes from high resolution intrinsic optical imaging spectroscopy (OIS). Quantified cortical layer profiling is demonstrated to be in agreement between VASO and contrast enhanced fMRI (using monocrystalline iron oxide nanoparticles, MION). Responses show high spatial localisation to layers of cortical processing independent of confounding large draining veins which can hamper BOLD fMRI studies, (depending on slice positioning). Thus, a cross species comparison is enabled using VASO as a common measure. We find increased VASO based CBV reactivity (3.1 ± 1.2 fold increase) in humans compared to rats. Together, our findings confirm that the VASO contrast is indeed a reliable estimate of layer-specific CBV changes. This validation study increases the neuronal interpretability of human layer-dependent VASO fMRI as an appropriate method in neuroscience application studies, in which the presence of large draining intracortical and pial veins limits neuroscientific inference with BOLD fMRI.

## 1. Introduction

The layered architecture of the cerebral cortex was first identified several centuries ago. The hierarchical structure of the cortex has since been parcellated based upon cell type, and the density of either cell bodies (Brodmann, 1909; Economo and Koskinas, 1925) or myelinated fibres (Smith, 1907; Vogt and Vogt, 1919). It is noted that the layering schemes based upon cyto- or myeloarchitecture methodologies do differ (Lashley and Clark, 1946); and modern delineation of layer boundaries now follow a multiparametric approach (Schleicher et al., 2005). While the definition of laminar borders moves towards statistical inference, it is widely accepted that the laminar organisation of cells and associated afferents is central to cortical function (Douglas and Martin, 2004a); with feed-forward and feedback pathways having known layer-specific termination patterns (Douglas and Martin, 2004b; Larkum et al., 2018). Non-invasive imaging of layer dependent functional activity supplements our understanding of structural parcellation and will result in a rapid increase of our knowledge of the working human brain.

Technological advances in MRI, both in terms of magnetic field (Polimeni and Uludağ, 2018), imaging gradient coil strength, detection hardware and advanced sequence designs (Poser and Setsompop, 2018), have permitted high resolution, in-vivo imaging of cortical anatomy (Trampel et al., 2019; Turner, 2013). Conventional MR measurements do indeed reflect the cortical architecture found in earlier histological studies (Eickhoff et al., 2005). The recent marriage of such data with methodological advances in quantitative MRI (based on phase contrast (Duyn et al., 2007) and diffusion (Assaf, 2019; Leuze et al., 2014) weighted imaging) delivers robust mapping of cortical layer structure.

* Corresponding authors.
*E-mail addresses:* renzohuber@gmail.com (L. Huber), aneurin.kennerley@york.ac.uk (A.J. Kennerley).
[1] Contributed equally.

https://doi.org/10.1016/j.neuroimage.2021.118195.
Received 24 July 2020; Received in revised form 17 May 2021; Accepted 19 May 2021
Available online 24 May 2021.

However, complementary mapping of brain function across the cortical layers with Blood Oxygenation Level Dependent (BOLD) functional (f)MRI, falls behind. A major reason for this is that conventional 2D gradient-echo (GE) BOLD measurements are confounded by signals originating from the large draining veins, driven by both large magnetic susceptibility effects and magnetic field angle dependence (Chu et al., 1990; Fracasso et al., 2018; Gagnon et al., 2015). Thus functional maps, while locally specific, show signals spreading across cortical layers and columns (Kennerley et al., 2005; Turner, 2002). To overcome these limitations and approach the mesoscopic spatial regime of cortical layers for brain function, alternative non-BOLD quantitative contrast mechanisms are required (Chai et al., 2019; Huber et al., 2019) in combination with modern hardware and readout regimes (Norris and Polimeni, 2019; Yacoub and Wald, 2018) - akin to the advances in structural based imaging. While an extensive range of techniques exists (e.g. GRASE Feinberg et al., 2008; Oshio and Feinberg, 1991, ASL Ivanov et al., 2016, SSFP Goa et al., 2014; Scheffler et al., 2018, functional diffusion Truong and Song, 2009, phase-sensitive fMRI Menon, 2002; Vu and Gallant, 2015 etc); one of the fastest growing approaches for layer-based fMRI utilises slice-saturation slab-inversion vascular space occupancy (SS-SI VASO) (Huber et al., 2014b). The VASO contrast exploits the difference between longitudinal relaxation times ($T_1$) of tissue and blood (Lu et al., 2003). Contrast is generated by applying a magnetization inversion pulse before signal acquisition, to effectively null the contribution of blood water pool at the time of signal excitation, while maintaining substantial tissue signal for detection. Thus, decreases in MR signal intensity during neuronal activity reflect the associated hemodynamic increase in the volume fraction of blood (or cerebral blood volume, CBV) (Attwell and Iadecola, 2002) within the imaged voxel.

VASO-based CBV measurements are particularly attractive for layer-specific functional brain imaging in humans because theoretically the method:

I offers a quantitative measure, being described in meaningful physical units (ml);
II it is believed to be insensitive to large draining veins (Jin and Kim, 2006; 2008; Lu et al., 2013);
III promises a more robust pseudo-measure of neuronal activity, maintaining signal change even in light of significant physiological changes (which have been demonstrated to dramatically affect BOLD fMRI (Kennerley et al., 2012a)).

Slice selective slab-inversion (SS-SI) VASO is widely used across the literature for non-invasive imaging of micro-vascular layer-specific signal responses (Beckett et al., 2020; Chai et al., 2019; Finn et al., 2019; Guidi et al., 2016; Kurban et al., 2020; Persichetti et al., 2020; Yang and Yu, 2019; Yu et al., 2019).

Although SS-SI-VASO is recognised as a powerful tool for layer-based fMRI studies, the 'exact' signal mechanisms remain enigmatic. Indeed over the last decade, much focus and debate has centred on enhancing our understanding of the VASO signal source (Donahue et al., 2006; Hua et al., 2009; Jin and Kim, 2006; 2008; Scouten and Constable, 2007; 2008; Uh et al., 2011; Wu et al., 2010). While the inverse relationship between VASO contrast and cerebral blood volume (CBV) changes has been partially validated, with Positron Emission Tomography (Uh et al., 2011) and contrast agent enhanced MRI (Jin and Kim, 2006; 2008; Lin et al., 2011; Lu et al., 2005), it is important to note that some of these comparison studies were of low spatial resolution (e.g. $3 \times 3 \times 3$ mm$^3$), used excessive smoothing filters, ignored some of the more interesting temporal dynamics of the response, and were based on non-quantitative correlative analysis. VASO contrast could be confounded by the complex interplay between cerebral blood volume, flow and extravascular BOLD effects (with inflow of fresh spins and partial volume effects further confounding measurement) (Donahue et al., 2006). Thus, the high correlations between VASO and alternative imaging methods may be erroneously dominated by these non-CBV components. Also, the layer-specific application of the VASO contrast remains unvalidated. The missing validation with gold standard methods might limit the wider uptake of the SS-SI VASO method for high-resolution fMRI.

To investigate whether the layer-dependent VASO response is indeed directly driven by stimulus induced changes in CBV, there is an urgent need for improved validation studies with particular focus on signal quantification (in physical units of ml) and detailed study of the signal contribution from large veins. While the insensitivity of high resolution layer-based VASO contrast to large draining vein effects has been qualitatively compared with standard GE-BOLD (reviewed in Huber et al., 2019), it has not been quantitatively validated with independent 'ground-truth' CBV imaging modalities to date.

Here we cross-validate layer-dependent VASO fMRI contrast with well established (but invasive) high resolution imaging methods (both optical and $Fe^{3+}$ contrast based CBV-weighted MRI) in a pre-clinical rat model in response to neuronal activation (somatosensory cortex) and respiratory challenge (hypercapnia). The leading hypothesis is that these independent methodologies will offer a deeper understanding/corroboration of the signal source of VASO contrast across the cortical layers; and permit in-depth study of the interspecies differences in VASO contrast. Optical imaging spectroscopy allows the assessment of haemoglobin concentration changes (in the two oxygenation states; summed to give total haemoglobin); while CBV-weighted VASO MRI actually assesses the $T_1$ component of the total blood volume. This study uses our specialised concurrent imaging based approach (Kennerley et al., 2012b) for improved and direct comparison between methodologies.

As alluded to above, when considering CBV fMRI contrast there are known interspecies differences which raise debate across the fMRI research field. There are two specific features of pre-clinical CBV-weighted fMRI that have not been confirmed in equivalent human studies to date. These discrepancies concern i) the absolute magnitude of CBV changes and ii) the overall temporal dynamics. Human CBV sensitive VASO fMRI studies find blood volume changes in the order of 30%–90% (compared to $CBV_{rest}$) in response to both visual and sensorimotor based neuronal activation (Donahue et al., 2006; Gu et al., 2006; Hua et al., 2009; Huber et al., 2014b; Lu et al., 2003; 2004b; 2004c; Poser and Norris, 2007; Scouten and Constable, 2008; Shen et al., 2009). Comparable animal studies with invasive methodologies report much smaller CBV changes of 10%–20% (Mandeville et al., 1998), ≈ 5%–8% (Kennerley et al., 2005), 5% (Kennerley et al., 2012a), and 4%–7% (Lu et al., 2004b) across a broad range of somatosensory stimuli and associated durations. Independent of such divergences in absolute CBV change, time course dynamics are also often qualitatively different between human VASO studies and equivalent measures reported across the animal literature. Human VASO studies suggest a fast recurrence to baseline of CBV after stimulus cessation (in the range of 10–15 s) (Hua et al., 2011; Lu et al., 2004; Poser and Norris, 2007; van Zijl et al., 2012), while rat data demonstrates delayed compliance (with a post-stimulus signal return to baseline in the order of 30–60 s) (Kennerley et al., 2005; Kida et al., 2007; Kong et al., 2004; Mandeville et al., 1999).

It can be argued that the interspecies differences in CBV amplitude and temporal dynamics (outlined above) reflect i) obvious methodical differences and thus signal source confounds, ii) task related and natural response differences, or simply iii) unavoidable anesthesia-dependent confounds in pre-clinical models. Extensive studies have suggested that anesthesia can 'slightly' reduce the overall response amplitude, but use of these agents cannot explain the temporal CBV dynamic differences between animals and humans (Berwick et al., 2002; Martin et al., 2006; Sicard et al., 2003; Zong et al., 2012). An extensive interspecies VASO contrast comparison between humans and animals, underpinned with data from more invasive imaging methods in the latter model, will help resolve these differences and aid our interpretation of the VASO fMRI signal source. VASO fMRI is a non-invasive contrast, which can easily be applied both in rats and in humans. Here we will investigate the haemodynamic response to stimulation of the primary somatosensory region of both the human and rat cortex (subsequently avoiding

potential brain region confounds). In addition we will investigate CBV changes in response to hypercapnic respiratory challenges. It is hypothesised that similar hemodynamic control pathways in humans and rats exist for such challenges (Mortola and Lanthier, 1996), enabling quantitative comparisons (after controlling for body mass and baseline blood oxygen saturation (Gray and Steadman, 1964)). Despite initial VASO comparisons with CBV-weighted fMRI at high spatial resolution in monkey visual cortex (Goense et al., 2012; Huber et al., 2014a) and cat visual cortex (Jin and Kim, 2006; 2008), the above described difference of response magnitudes between VASO and non-VASO CBV imaging have not been resolved to date.

The present study therefore aims to investigate the cortical layer based sensitivity of VASO-derived CBV measurements in both human and rat models. VASO insensitivity to changes in the large draining veins on the cortical surface will be confirmed in rodents by direct comparison of functional changes (to neuronal activation/hypercapnia) acquired by VASO, contrast enhanced/CBV weighted fMRI and BOLD fMRI, with concomitantly acquired optical measures of total haemoglobin and blood oxygenation. Data will be used to validate the layer-dependent CBV profile of VASO and contrast enhanced MRI within the same animals, within the same session. Ultimately, we seek to compare layer-dependent fMRI profiles of CBV and BOLD across rodents and humans using the same non-invasive SS-SI-VASO sequence in primary somatosensory cortex measured at the same MRI field strength (7 T). This high-resolution validation study of VASO contrast with an established preclinical model will be of particular interest to the growing field of high-resolution layer based fMRI; data will deepen understanding of the VASO fMRI signal source and help increase the wider uptake of the SS-SI-VASO method.

## 2. Methods

Here we implement VASO based fMRI in a preclinical model utilising concurrent intrinsic optical imaging techniques (Kennerley et al., 2005) (developed over 15 years ago) to investigate the underlying haemodynamics with high spatio-temporal resolution.

VASO, as a potential measure of cerebral blood volume changes in response to neuronal activation, was originally developed for use in the human brain at low magnetic fields (1.5 T) (Lu et al., 2012). Unfortunately, as magnetic field strength increases the $T_1$ relaxation time constants for intravascular and extravascular compartments converge (Jin and Kim, 2008); and thus contrast to noise between nulled and non-nulled signals decreases. To account for this convergence and make the VASO sequence viable (in terms of contrast to noise) at higher field strengths (7T+), a variant SS-SI VASO pulse sequence was previously introduced (Huber et al., 2014b). For application in an animal model at high fields (7T+), distinct features in physiology (e.g. short arterial arrival time (Calamante et al., 1999)) and associated magnetization dynamics must be reconsidered. Due to the fast heart rate in rat models, there is increased risk of inflow of non-inverted blood magnetization into the imaging slice during the blood nulling time, and thus if unaccounted for, VASO signal can become unreliable (Hua et al., 2013) as steady state magnetisation is impaired (Donahue et al., 2009). To correct for this difference, additional modules to control the magnetization were introduced to the SS-SI-VASO sequence here. These include implementation of additional slice-selective and global spin-reset saturation pulses to account for the different z-magnetization relaxation histories (steady-state) of stationary tissue and blood flowing into the imaging slice (Hua et al., 2013; Lu, 2008). This is used to increase functional contrast to noise and avoid contamination of changes in CBF. One repetition time (TR) of the adapted SS-SI-VASO sequence is depicted in Fig. 1A.

In order to minimize the sensitivity to potential dynamic changes in CSF (Donahue et al., 2006; Jin and Kim, 2010; Piechnik et al., 2009; Scouten and Constable, 2008), we followed a previous approach using a combination of flip angle, TIs and TRs that make GM and CSF appear

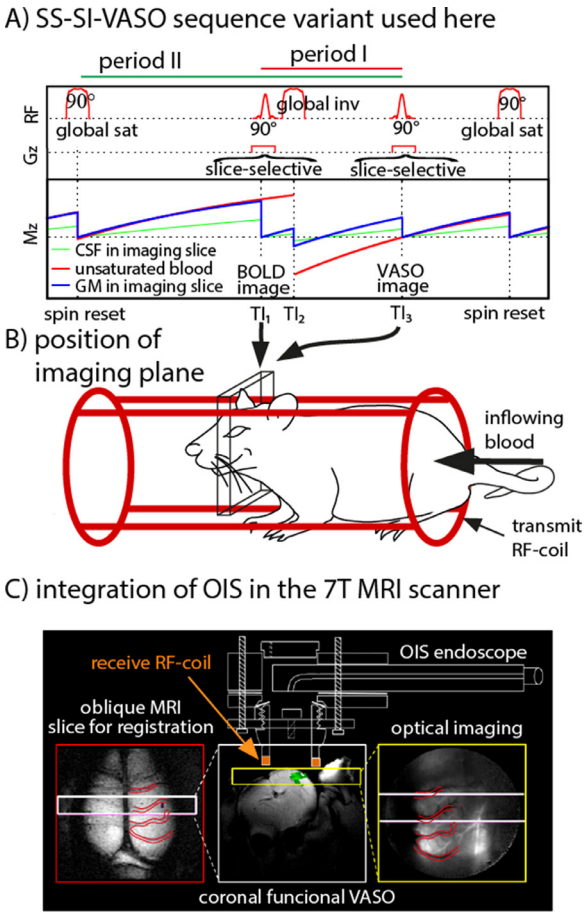


**Fig. 1. Acquisition procedure of SS-SI VASO used in rats to account for the faster arterial arrival time compared to humans.** Acquisition procedure of SS-SI VASO in rats: **A)** depicts a pulse sequence diagram of SS-SI VASO modified for application in rodent brains at high fields (7T+). Before every TR, a global adiabatic saturation pulse is applied, ensuring control of the magnetization steady-state across the parts of the animal covered by the large quadrature volume resonator. This global reset pulse shortens the time that the flowing blood pool magnetization requires to transition into a steady-state. In-plane magnetization is saturated by a slice-selective 90° excitation pulse prior to the acquisition of a BOLD weighted image ($TI_1$; without blood nulling). After this saturation pulse, a global inversion pulse is applied ($TI_2$) and subsequent VASO signal acquisition performed at the blood-nulling time $TI_3$. **B)** depicts the approximate position of slice-selective saturation and 'global' inversion pulses. A large 180 mm inner diameter quadrature coil is used to ensure inversion across the body and enable concurrent optical imaging setup. **C)** depicts a schematic illustration of our concurrent fMR and intrinsic optical imaging spectroscopy (OIS) setup and acquisition planes. Concurrent optical imaging inside the bore of the scanner is permitted through a non-magnetic medical endoscope. The apparatus to hold the endoscope in place is surgically attached to the cranium and has a built-in surface coil for MR RF reception. The large draining veins are visible in both $T_2^*$ weighted MR images and corresponding high- resolution optical images. Such vascular landmarks help co-register data between the imaging modalities.

at similar signal intensities (more details in Huber et al., 2015; Huber et al., 2014b; Huber et al., 2014c).

Before every TR, a global adiabatic 90° spin-reset pulse is applied to eliminate the spin history of all magnetization pools (e.g. stationary tissue, nulled/un-nulled blood etc.) within the 1H quadrature resonator (Bruker 1P-T9561, 300MHz, 1kW max, 200/180 mm OD/ID) used for RF transmission (Fig. 1B). The amplitude and phase shape-functions of this radio-frequency pulse were adapted from the TR-FOCI pulse class, designed for use at 7 T (Hurley et al., 2010). In order to convert the original TR-FOCI pulse from an inversion pulse to a 90° saturation pulse,

a 90° phase skip of the pulse amplitude was introduced half-way through the pulse duration, resulting in an inversion efficiency of 50%, despite the $B_1$ inhomogeneities of the transmit coil (Mispelter et al., 2006). A more detailed description on the operating principle of this RF pulse can be found in (Huber et al., 2014b). All blood in the imaging slice is expected to be nulled to provide a pure VASO contrast, when two assumptions are fulfilled: firstly, the microvasculature of the imaging slice is refilled during period I (Fig. 1A)- blood velocity and transit time measurements suggest that the microvasculature of a 2 mm imaging slice is refilled in less than 1.5 s (Hutchinson et al., 2006; Ivanov et al., 1981; Kennerley et al., 2010; Kim and Bandettini, 2010; Kleinfeld et al., 1998; Pawlik et al., 1981)–and secondly, no fresh (uninverted) blood from the hindquarters of the animal flows into the imaging slice during period II (Fig. 1A).

### 2.1. Experimental setup for data acquisition in rats

All aspects of these concurrent imaging methods and their development have been previously described (Kennerley et al., 2012b). A brief description is given here for completeness. All experiments were performed with UK Home Office approval under the Animals (Scientific Procedures) Act of 1986. Female hooded Lister rats (total n = 5) weighing (250–400 g) were kept in a 12 h dark/light cycle, at a constant temperature of 22 °C, with food and water ad libitum. Animals were anesthetized (i.p. urethane 1.25 g/kg) with additional 0.1 ml doses administered as necessary. A single subcutaneous injection of Atropine (0.4 mg/kg) reduced mucous secretions throughout the experiment. Rectal temperature was maintained at 37 °C throughout surgical and experimental procedures using a homeothermic blanket (Harvard Apparatus Inc, USA). Animals were tracheotomized to allow artificial ventilation and permit controlled respiratory challenges. Ventilation parameters were adjusted to maintain blood gas measurements (measured via blood letting) within physiological limits (pO2 = 105 mm Hg ± 4; pCO2 = 38 mm Hg ± 5). Left and right femoral veins and arteries were cannulated. Phenylephrine (0.13–0.26 mg/h) was infused i.v. to maintain blood pressure (measured via pressure transducer connected to the arterial cannulae - CWE systems Inc. USA) between physiological limits (MABP, 100–110 mm Hg (Nakai and Maeda, 1999)).

Intrinsic optical imaging in rat models is an invasive methodology requiring direct access to the cortex for spectroscopic analysis of remitted light (Lieke et al., 1989; Mayhew et al., 1999). To facilitate this, animals were placed in a stereotaxic frame (Kopf Instruments, USA). The skull overlying the right somatosensory cortex was thinned to translucency with a dental drill under constant cooling with saline. A bespoke single loop RF surface coil, integrated into a 20 mm diameter Perspex well was fixed to the animals' head using dental cement, ensuring that the thin window lay in the centre of the well. This well is used to both secure the animal inside the MRI scanner and also holds the non-magnetic endoscope (Endoscan Ltd, London) used to permit concurrent optical imaging of the cortex within the magnet bore (Fig. 1C). The well is filled with deuterium oxide ($D_2O$) to i) reduced optical specularities from the skull surface (for optical imaging); and ii) reduce air-tissue susceptibility artefacts (around the thinned cranial window for high field fMRI) whilst being MR silent at the proton resonant frequency.

Platinum electrodes, insulated to within 2 mm of the tip, were inserted, in a posterior direction, between whisker rows A/B and C/D of the left whisker pad, ensuring the whole pad received activation following electrical stimulation.

The animal was placed inside a 7 T small bore MRI scanner (Bruker BioSpec Avance II, 70/30, Bruker Biospin GmbH, Ettlingen, Germany) with preinstalled, actively shielded, 200 mm inner diameter, water cooled, gradient coil (Bruker BioSpin MRI GmbH B-GA20. 200 mT/m maximum strength per axis with 200 μs ramps). Inside the magnet bore an electrically filtered and isolated heating blanket (Harvard Apparatus Inc. USA), and rectal probe, maintained body temperature. The animal was artificially ventilated (Zoovent Ltd, UK) with medical grade air and breathing rate measured using a pressure sensitive pad (SAII, USA – Model 1025L Monitoring and Gating System). Standard FLASH based imaging was used to guide subsequent positioning of the fMR imaging plane.

SS-SI-VASO as described above was implemented in Paravision V running Topspin 3.1 (Bruker). Image sequence parameters were $TR/TI_1/TI_2/TI_3/TE$ = 3200/1100/1500/2530/10 ms respectively. A 2 mm thick coronal imaging slice covering most of the somatosensory whisker barrel cortex (centred based on known stereotaxic coordinates: 3 mm posterior to bregma based on an axial image of the dorsal surface of the brain);; with field of view 30 × 30 $mm^2$ and matrix size 64 × 64 (in-plane resolution ≈ 470 μm) was used. Use of a coronal imaging plane ensures that the blood refilling conditions (discussed above) are fulfilled and enables depth profiling of response through the cortex.

Intrinsic optical imaging spectroscopy is a well-established technique for delivering high resolution, spatially resolved maps of changes in total haemoglobin (HbT) and oxygen saturation (Chance, 1991) (and subsequently deoxy- and oxy-haemoglobin, Hbr and $HbO_2$ respectively). A switching galvanometer system (Lambda DG-4 Sutter Instruments Company) with 4 wavelength filters ($\lambda$ – 495 ± 31, 587 ± 9, 559 ± 16 and 575 ± 14 nm) was used to illuminate the cortex through the medical endoscope. A CCD camera running at 32 Hz (8 Hz effective frame rate for each wavelength) captured remitted/reflected light images with an in-plane spatial resolution of ≈ 80 μm × 80 μm. Light attenuation in response to a stimulation event was calculated and subsequent spectral analysis utilised a modified Beer–Lambert law approach. Under differential Beer-Lambert law analysis resultant changes in light absorption, and therefore HbT, remain relative in units of percent changes. Mean differential pathlength was estimated using Monte Carlo simulations of light transport through a parameterised heterogeneous tissue model (Kennerley et al., 2009; 2012b). To encode depth information this heterogeneous model accounted for baseline changes in cerebral blood volume and oxygenation saturation across the cortical depth (estimated from MR priors previously described and based on a mean of 106 μm and 50% respectively). The approximate depth at which saturation and volume changes occur is also a free parameter. Resultant 2D maps of concentration changes in $HbO_2$, Hbr and HbT, alongside raw optical images of the cortical surface aid positioning and cross-validation of image geometry to MRI based on large veins, clearly visible in both modalities (Fig. 1C).

Concurrent OIS and VASO based fMRI data was recorded in response to 16 s electrical stimulation of the whisker pad (5 Hz, 1.2 mA). In all experiments, an initial baseline of 60 s was collected, followed by fifteen stimulation events, each with an inter-stimulus interval (ISI) of 86 s. Additional functional experiments used hypercapnic respiratory challenge. Trials were 9 min in duration, consisting of 2 min baseline (medical air), 5% increased $FiCO_2$ for 5 min, and a further 2 min baseline. Trials were repeated 12 times to increase CNR.

Following completion of the VASO fMRI experiments, 10 mg/kg of a monocrystalline iron oxide nano-compound (MION) contrast agent (AMI-227 Sinerem; Guerbet Laboratories) was infused intravenously. Infusion took place over 1 hr in steps of 0.1–0.8 ml, a total equivalent to 160 μM concentration and allowed quantification (via high resolution $T_2^*$ weighted imaging - 256 × 256 pixels, FOV = 30 mm, slice thickness = 1 mm, TR/TE = 1000/15 ms, flip angle = 90°, 2 averages) of baseline blood volume fraction following (Troprès et al., 2001).

All electrical whisker stimulation experiments were repeated after full injection of the contrast agent, to measure MR based changes in CBV following Mandeville et al. (1998). Functional data were acquired using single shot GE-EPI (raw data matrix = 64 * 64, FOV = 30 mm, slice thickness = 2 mm, TR/TE = 1000/12 ms, flip angle 90°, 10 dummy scans). In order to account for BOLD contributions in MION results, we normalized the functional signals pre- and post-contrast injection. By completing concurrent 2D-OIS with BOLD, CBV, and $CBV_{rest}$, we have a comparative measure unaffected by the contrast agent for normalization.

Preliminary accounts of the rodent data of this study have been previously shown as auxiliary material for validating human VASO signal characteristics. Namely, representative MION and VASO fMRI data of this study were shown in panel c-d of Fig. 6 in (Huber et al., 2015) as well as a full description of all animals in the conference proceedings ISMRM 2020 (Kennerley et al., 2020). Preliminary accounts of the VASO and OIS comparisons were described in the conference proceedings of ISMRM 2013 (Kennerley et al., 2013).

### 2.2. Experimental setup for data acquisition in humans

Data for human experiments were acquired cross-centre (see below), on MAGNETOM 7 T scanners (Siemens Healthcare, Erlangen, Germany) using the vendor-provided IDEA environment (VB17A-UHF). For RF transmission and reception, identical single-channel-transmit/32-channel receive head coils (Nova Medical, Wilmington, MA, USA) were used. All scanners used were equipped with a SC72 body gradient coil. Informed written consent was given by all participants.

Human hypercapnia data (n = 5) were acquired at the Max Planck Institute for Human Cognitive and Brain Sciences in Leipzig, Germany. These procedures for human volunteer scanning with respiration challenges were approved by the ethics committee of the University of Leipzig. Respiratory challenges to induce hypercapnia in humans were matched to the design implemented in the rodent experiments e.g. 2 min breathing air, 5 min breathing 5% increased $FiCO_2$, and 2 min breathing air again.

Somatosensory stimulation data (n = 9) using abrasive cushions were acquired at SFIM at NIH, Bethesda USA under an NIH Combined Neuroscience Institutional Review Board-approved protocol (93-M-0170) in accordance with the Belmont Report and US Federal Regulations that protect human subjects (ClinicalTrials.gov identifier: NCT00001360). Tapping-induced somatosensory activation followed the same task timing as the rodent experiments (16 s activation with 86 s ISI) but with only 12 repeats (total run duration 18 min 12 s). The task consisted of pinch-like finger tapping and passive touching with an abrasive cushion. The participants were instructed about the task timing inside the scanner bore via a projector and mirror system.

Somatosensory stimulation data (n = 3) using brushes and piezoelectric vibration were acquired at Scannexus (Maastricht, The Netherlands), the corresponding procedures having been approved by the Ethics Review Committee for Psychology and Neuroscience (ERCPN) at Maastricht University, following the principles expressed in the Declaration of Helsinki. Three different stimulation tasks were deployed i) finger tapping, ii) passive finger brushing, and iii) passive somatosensory stimulation delivered by a piezoelectric vibrotactile stimulation device (mini PTS system, Dancer Design, UK). All tasks involved the left index finger and thumb. For the passive stimulation, a ceramic mini-PTS stimulator module was held by the participant between the left index finger and thumb. The stimulator module houses a vertically moving aluminium disk (diameter: 6 mm) centered in a static aperture (diameter: 8 mm), delivering a 25Hz vibrotactile stimulus (30s with random 'silent' intervals to prevent habituation). The maximum mechanical power delivered to the skin was 75mW (corresponding to a disk movement within the range of 0.5 mm). All stimulation scripts are available for PsychoPy v2.0 and for Presentation v16.1 on Github (https://github.com/layerfMRI/Phychopy_git/tree/master/TappingWithTrTiming and https://github.com/layerfMRI/Phychopy_git/tree/master/Piezo/S1ANFUNCO).

Experimental parameters for VASO data acquisition across the experimental paradigms above followed (Huber et al., 2014b) and were inline with the rodent experiments. In short, to account for short arterial arrival time, the inversion efficiency was reduced to 75%. Further sequence parameters were $TR/TI_1/TI_2/TE$ = 3000/765/2265/19 ms. For the hypercapnia data nominal resolution was $1.5 \times 1.5 \times 1.5$ $mm^3$. For laminar comparisons of CBV change in S1, in response to somatosensory stimulation, higher-resolution experiments (Huber et al., 2020b; 2017) were performed with nominal in plane resolution of $0.75 \times 0.75$ $mm^2$ and slice thickness of 0.7–1.8 mm.

### 2.3. General VASO-based data analysis

All fMRI time series were analysed with standard layer-fMRI VASO procedures, as explained in multiple previous publications (Huber et al., 2020a; 2020b; 2017; 2014b) and our accessible open source online tutorials (https://layerfmri.com/analysispipeline/). In short, time-resolved image repetitions were motion corrected using SPM12 (UCL, UK) (Penny et al., 2007). Volume realignment and interpolation were performed with a 4th-order spline. In order to minimize effects of variable distortions (non-rigid motion), the motion was estimated in a brain mask generated in AFNI (Cox, 1996).

Raw VASO data consisted of interleaved acquisitions of MR signal with and without blood nulling (corresponding to CBV and BOLD weighted images). To eliminate unwanted contamination of extravascular BOLD signal within the extracted VASO contrast images the analysis pipeline treated odd and even time points separately for the motion correction and subsequently divided the resultant images by each other (Huber et al., 2014b).

For both rodent and human data, the ensuing layer-dependent signal sampling required manual estimation (based upon $T_1$-weighted EPI data) of boundary lines between the grey matter (GM) ribbon, cerebrospinal fluid (CSF) and white matter (WM) to account for cortical curvature. A coordinate system across cortical layers[2] and columnar structures were estimated in LAYNII (https://github.com/layerfMRI/LAYNII). LAYNII is an open source C++ software suite for computing layer functions (Huber et al., 2021). We estimated the depth of equivolume distributed layers (Waehnert et al., 2014). With the resolution of 0.47-0.75 mm, we obtained 4–8 independent data points across the thickness of the cortex. Across these data points, we created 11 layers[3] across the thickness of the cortex (≈2mm for both human and rat somatosensory cortex) on a 4-fold finer grid than the effective and nominal resolution.

For hands-on tutorials for user friendly acquisition and analysis procedures as employed in this study see: (https://layerfmri.com/analysispipeline/ and https://youtu.be/PngT6chFy6c).

### 2.4. Quantification of relative and absolute CBV with MION

Signal changes due to susceptibility arising from intravascular contrast agents can be described with the formalism given in (Kim et al., 2013; 2007; Troprès et al., 2001; Zhao et al., 2006):

$$\frac{S(d')}{S(d=0)} = \frac{S_{rest} e^{-\frac{4}{3}\pi\gamma B_0 \Delta\chi(d')CBV\ TE}}{S_{rest} e^{-\frac{4}{3}\pi\gamma B_0 \Delta\chi(d=0)CBV\ TE}}. \quad (1)$$

Here, $S_{rest}(\rho, T_2^*$, etc.) contains signal parameters that are independent of iron oxide contrast agent injected, $d$ is the relative dose of contrast agent in randomly orientated cylindrical vessels (Yablonskiy and Haacke, 1994), and assuming that $CBV \ll 1$, and $TE \gg \frac{1}{\delta\omega}$ (Troprès et al., 2001). Note that $CBV$ refers to the relative blood volume in units of ml per ml of tissue. Contrast agent induced susceptibility change $\Delta\chi(d') \approx 0.571\text{ppm} \times d'$ can be taken from the literature (Kennerley et al., 2005; Troprès et al., 2001). Equation (1) can be rewritten as:

$$\frac{S(d')}{S(d=0)} \approx e^{-\Delta R_2^*(d')TE}, \text{ where} \quad (2)$$

[2] Note on terminology: In the context of fMRI, these estimates of cortical depth do not refer to cytoarchitectonically defined cortical layers (https://layerfmri.com/terminology).

[3] The number of eleven layers was chosen based on previous experience in finding a compromise between data size and smoothness (https://layerfmri.com/how-many-layers-should-i-reconstruct).

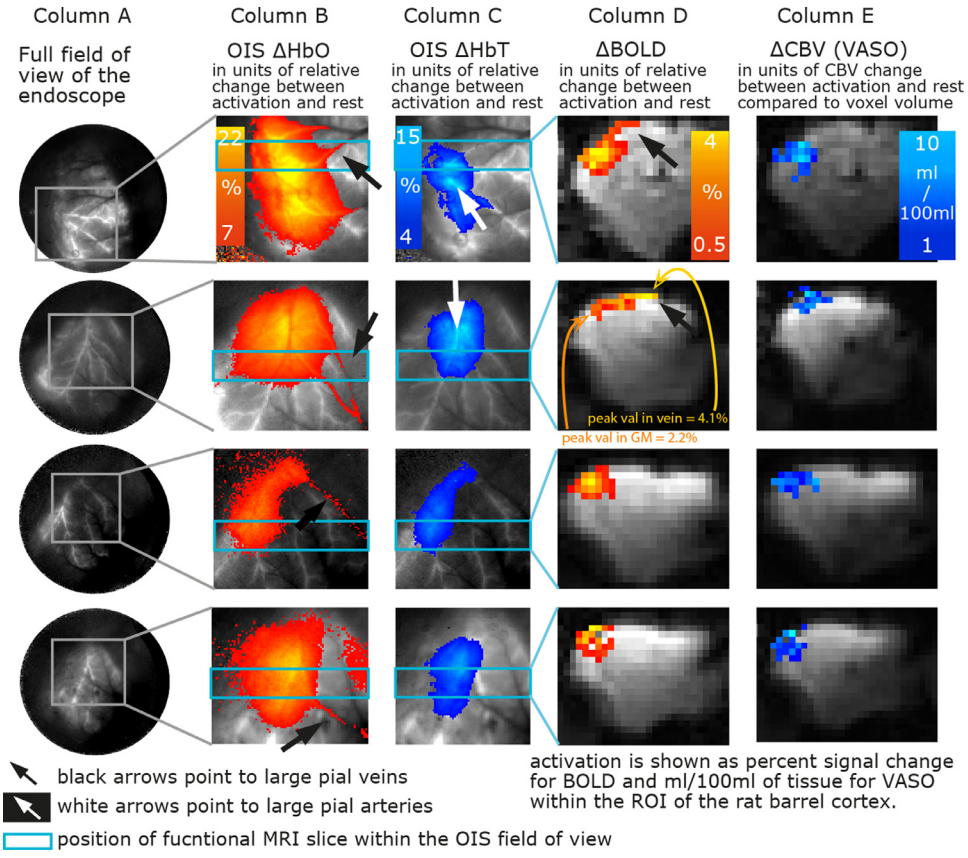


**Fig. 2. OIS and fMRI activation maps of four animals.** Data here shows that VASO-CBV contrast is not sensitive to the large draining veins, which are clearly visible in OIS $\Delta HbO_2$ and fMRI ΔBOLD activation maps. The VASO CBV response is observed to be specific to the whisker barrel cortex, similar to OIS measures of ΔHbT. Each row depicts one individual animal. **Column A)** depicts the total FOV of the non-magnetic endoscope used to enable concurrent imaging. The grey scale here references HbT response to $C_{O2}$-induced hypercapnia. Note, arterial vessels are bright, brain tissue is grey, and pial veins display dark contrast. This contrast is used as an underlay/reference image for the somatosensory stimulation results shown. **Columns B)-C)** depict OIS estimates of $\Delta HbO_2$ and ΔHbT. Draining veins show strong changes in $\Delta HbO_2$, distant from activated tissue (black arrows). HbT changes, however, are confined to activated tissue. Pial arteries are clearly a major contributor to the HbT change (white arrows). **Columns D)-E)** depict coronal BOLD and CBV fMRI slices extracted from VASO. In animals where the fMRI slice covered the large pial veins (top rows), significant BOLD signal change distal of the barrel cortex (and highest CBV change) was observed (black arrows). Such signals are attributed to venous BOLD weighting amplified by the vessel orientation to the main static magnetic field.

$$\Delta R_2^*(d') \approx \frac{4}{3}\pi\gamma B_0 \Delta\chi(d') CBV. \tag{3}$$

While in many applications $\Delta R_2^* \ll TE$ and the relative signal change is assumed to be linear dependent on the susceptibility, at high magnetic fields or in voxels with very short $T_2^*$, this is not completely valid and the decay must be considered to be exponential as shown in Eq. (2). Based on the measured change in $R_2^*$, Eq. (2) can be used to estimate $CBV$:

$$CBV = \frac{\Delta R_2^*(d)}{\frac{4}{3}\pi\gamma B_0 \Delta\chi(d)}. \tag{4}$$

This means that the absolute CBV can be converted from the measured MR signal as:

$$CBV = \frac{ln\left(\frac{S_{pre\ contrast}}{S_{post\ contrast}}\right)}{-\frac{4}{3}\pi\gamma B_0 \Delta\chi(d) TE}. \tag{5}$$

Contrast doses are usually in the range of 10 mg/kg (10 mg/kg in this study) to have a maximum contrast with minimum intravascular signal, but to still have enough extravascular signal left for acquisition. In order to minimize contaminations of susceptibility changes arising from the blood oxygenation level, measured signal intensities $S(d')$ and $S(d = 0)$ should refer to the same activation state. This means that for one measurement of activity induced $CBV$, two experiments must be conducted, one before contrast agent injection and one after contrast agent injection.

The absolute change of $CBV$ with MION is estimated by means of (5) as:

$$\Delta CBV = CBV_{act} - CBV_{rest} =$$

$$\frac{1}{\frac{4}{3}\pi\gamma B_0 \Delta\chi(d)}\left[ln\left(\frac{S_{pre}^{act}}{S_{post}^{act}}\right) - ln\left(\frac{S_{pre}^{rest}}{S_{post}^{rest}}\right)\right]. \tag{6}$$

The relative percent signal change of MION after BOLD correction is estimated as:

$$\frac{\Delta S}{S_0} = \frac{\left(\frac{S_{pre\ contrast}^{act}}{S_{post\ contrast}^{act}}\right) - \left(\frac{S_{pre\ contrast}^{rest}}{S_{post\ contrast}^{rest}}\right)}{\left(\frac{S_{pre\ contrast}^{rest}}{S_{post\ contrast}^{rest}}\right)}. \tag{7}$$

This way of estimating the absolute CBV change without the use of Taylor expansion is identical to the descriptions in (Troprès et al., 2001). Also preliminary presentations of the data in this study shown in (Huber et al., 2015) were quantified in this exact fashion. However, in preliminary presentations, the full mathematical formalism was not described and only a simplified description about the influence of baseline CBV was given.

## 3. Results

### 3.1. Concomitant OIS and VASO

VASO-derived CBV changes and BOLD fMRI maps are shown in Fig. 2, alongside optical measures of the underlying haemodynamics, in response to somatosensory stimulation of the whisker pad. Extracted ROI based time series are shown in Fig. 3. Quantitative estimates of changes in oxygenated haemoglobin(ΔHbO) and total blood volume (ΔHbT) can be made based on the parameterized baseline values (see methods). The sensitivity (in terms of CNR) of all modalities was high enough following trial averaging to detect activation changes in the primary somatosensory cortex. The large draining veins (visible in both structural MRI and raw/analysed OIS data) were used as fiducial markers to align the axial fMRI slice within the field of view of the optical endoscope (turquoise outlines in Fig. 2). Alignment confirmed that in two animals the barrel cortex (and thus the fMRI slice position) happened to overlap with large pial veins draining the primary somatosensory cortex

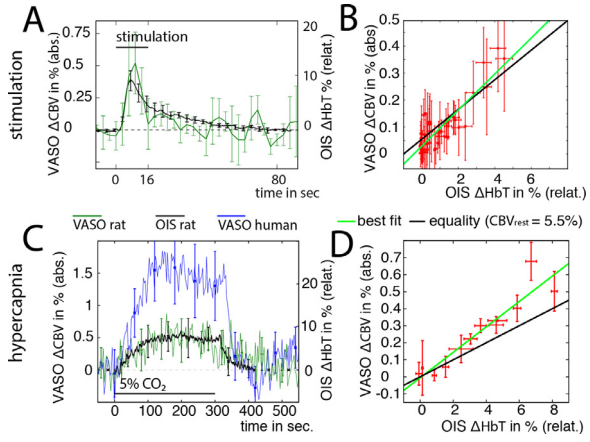


**Fig. 3. Comparison of OIS and VASO-CBV measurements in time.** Unique temporal characteristics of CBV and HbT responses to neuronal activation and respiratory challenges are explored. **Panels A)** and **C)** depict CBV and HbT time courses during somatosensory stimulation and hypercapnia, respectively. Human data time series for hypercapnia is shown for completeness (see Section 3.3). It can be seen that the time course dynamics between both modalities (VASO and OIS) are in agreement (within standard deviation error). Note that these time-courses show the unique feature of a slow return to baseline after neuronal activation (across a time scale of 80 s) without the post-stimulus undershoot typically observed in equivalent human data. Error bars reflect inter-subject standard deviation across participants. **Panels B)** and **D)** show the same data in the form of scatter plots. For the sake of clarity, individual points refer to the averaged signal of multiple adjacent time points. No hysteresis is observed. Data in panels A) and B) refer to ROIs in S1 only, while data in C) and D) refer to the total GM of the right hemisphere within one acquired slice. While both imaging modalities, VASO and OIS, respectively, provide estimates of change in units of %, the reference volume is not the same. Percent volume change in OIS refers to relative (relat.) stimulus-evoked volume changes compared to the volume estimates at baselines (without task). Percent volume change in VASO refers to absolute (abs.) stimulus-evoked volume changes compared to the volume of the imaging voxel (independent of the baseline CBV). Note that the VASO data presented here are shown in units of $CBV/CBV_{rest}$, by normalising the VASO present signal changes with an assumed average baseline $CBV_{rest}$ value of 5.5%. This normalisation was not done for VASO-MION comparisons in the remaining figures of this article.

of the rat brain (top two rows of Fig 2). A BOLD signal change extending away from the somatosensory cortex and towards the superior sagittal sinus is highlighted (black arrow). Interestingly, in one animal, this venous signal (4.1% at yellow arrow in Fig. 2) was greater in magnitude than the signal in the neurally active region within the somatosensory cortex (2.2% at orange arrow in Fig. 2). No corresponding venous signals extending away from the somatosensory cortex were observed in the CBV-based functional maps (even when different thresholds were set). It is noted that due to the position of the rodent head with respect to the static magnetic field the signal in the draining vein (at 90 degrees to the field) is most likely amplified due to the BOLD signal magnetic field angle dependence (Chu et al., 1990)

In contrast, in the two animals depicted in the bottom rows of Fig. 2, the fMRI slice position does not overlap with large pial veins. In such cases we observed that the activation 'extent' of both BOLD and CBV (based on VASO contrast) signal changes were spatially comparable.

In all cases, the optical estimates of total haemoglobin do not show enhanced sensitivity to large draining veins. Indeed HbT changes appear greater in pial arteries (white arrows). These macro-vascular arterial HbT responses are expected also to contribute to the overall layer-dependent activation profiles measured here. Thus, the final VASO and MION layer profiles are expected to reflect both macrovascular and microvascular CBV changes.

Time courses of induced changes in CBV (VASO) and HbT (optical) are shown in Fig. 3A, based on regions of interest drawn from the activation maps in response to somatosensory stimulation shown in Fig. 2. As shown, there is excellent temporal agreement between the two measures. The reader is reminded that OIS estimates HbT changes in relative percent changes (to an assumed 106 μM baseline (Kennerley et al., 2005)), while VASO estimates CBV changes in relative percent volume change compared to the voxel volume. To compare VASO and OIS reponses in the same *relative* units (of baseline blood volume), the VASO signal was normalized to a literature value baseline CBV, which is assumed to be 5.5% in GM. This value has been established across two decades of VASO history (Donahue et al., 2006; Gu et al., 2006; Hua et al., 2009; Huber et al., 2014b; Lu et al., 2003; 2004b; 2004c; Poser and Norris, 2007; Scouten and Constable, 2008; Shen et al., 2009). The somatosensory CBV changes in response to whisker stimulation peak in the range of 5%-10% (compared to the baseline CBV). Such amplitudes are consistent with previously reported ΔCBV estimates in the pre-clinical domain (Hillman et al., 2007; Kennerley et al., 2005; 2012a; Lee et al., 2001; Tian et al., 2010), whereas they are about 5–10 times smaller than previously reported VASO signal changes in humans (Beckett et al., 2020; Chai et al., 2019; Finn et al., 2019; Guidi et al., 2016; Kurban et al., 2020; Persichetti et al., 2020; Yang and Yu, 2019; Yu et al., 2019).

A scatter plot of group-averaged time points of HbT and CBV change measured via OIS and VASO respectively is shown in Fig. 3. The concurrent measures are within standard error of a 1:1 relationship across the whole time series (no hysteresis was observed). Cross modality comparisons of stimulus induced somatosensory activation are somewhat limited by the low sensitivity of VASO and correspondingly large error bars. It is noted that hypercapnia-induced CBV/HbT responses (which were higher in magnitude and longer lasting) yielded more reliable and consistent responses across animals (Fig. 3C-D). The time courses of OIS and VASO were very consistent and both exhibited a characteristic delayed compliance on return to baseline after trial cessation (in-line with Windkessel model predictions (Kida et al., 2007; Kong et al., 2004; Mandeville et al., 1999)).

### 3.2. VASO vs. MION derived CBV and associated cortical profiling

Layer-dependent responses of CBV change estimated with the SS-SI-VASO sequence were compared to layer-dependent responses of MION fMRI in the primary somatosensory cortex. Fig. 4 depicts the respective maps (panel A) of depth-dependent (f)MRI signals and the corresponding group-averaged functional layer-profiles (panels B-C). While GE-BOLD is dominated by the draining vein effect and shows the strongest functional signal changes at the cortical surface, VASO and MION based CBV responses are strongest inside the GM of the activated brain region. Neither CBV measure displayed confounding venous weightings.

When analysed in their native physical units of relative percent signal change, VASO and MION CBV profiles show diverging layer-profiles at the brain surface (pink arrow). The MION CBV profile is dominated by CBV changes in the deeper layers, consistent with previously reported MION-CBV layer profiles in preclinical studies (Goense et al., 2007; Kennerley et al., 2005; Kim and Ugurbil, 2003; Mandeville et al., 2001; Silva and Koretsky, 2002; Silva et al., 2007; Zhao et al., 2006). The VASO CBV profile, however, also exhibits a similarly elevated CBV response in the superficial layers. This is consistent with previous layer-fMRI VASO studies (Beckett et al., 2020; Chai et al., 2019; Donahue et al., 2017; Finn et al., 2019; Guidi et al., 2016; Huber et al., 2014a; 2015; 2017; 2016; Kurban et al., 2020; Persichetti et al., 2020; Yang and Yu, 2019; Yu et al., 2019) and might appear in conflict with the large body of preclinical studies. Note that the superficial activity in VASO profiles is located within the cortex and is approx. 0.8 mm deeper than the GE-BOLD peak response above the cortical surface. While the seemingly different CBV response of VASO and MION fMRI in the superficial layers was an unexpected finding in this study, it can be explained by the fact that the percent signal change of VASO and MION fMRI estimate CBV changes in different 'absolute' units (exponential vs. linear CBV dependence). When analyzed in the same quantitative physical units (ml

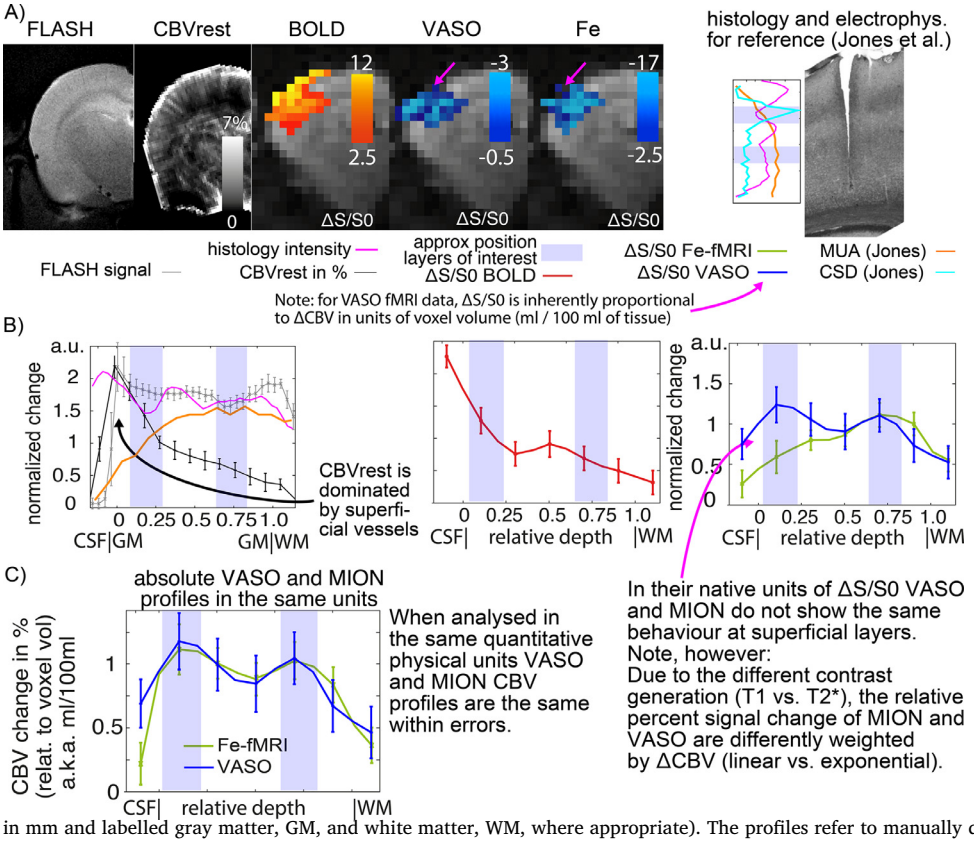


**Fig. 4. Comparison of CBV layer profiles in the rodent primary sensory cortex with VASO and MION.** Data shows that CBV changes estimated from functional VASO and MION maps show the same cortical layer profiles, when analysed in the same quantitative physical units. **Panel A)** depicts the coronal slices from the various MRI contrasts acquired through this study (from one representative animal). High-resolution FLASH data are used to estimate the approximate position of cortical layers (excitatory/inhibitory) (Narayanan et al., 2017). See also included electrophysiology and histology (cytochrome oxidase staining) data from Jones et al. (2004) for the position of the expected excitatory and inhibitory layers. The CSD spike (in rat) is quoted to relate to "primary sensory input from the thalamus" (first bump in the VASO profiles). The MUA peak deeper in the cortex is "likely to reflect the spiking activity of projection neurons in the deeper layers" (second bump in the VASO profiles). Functional activation maps refer to percent signal change of the respective contrast. The activation maps of BOLD signal change are dominated by voxels at the cortical surface (≈0 mm). Note that the superficial CBV change seems to be stronger in VASO activation maps compared to MION (pink arrow). **Panel B)** depicts the corresponding layer profiles of all the depicted MRI modalities in the form of profile plots (cortical depth in mm and labelled gray matter, GM, and white matter, WM, where appropriate). The profiles refer to manually drawn ROIs of the primary somatosensory cortex. Signals are averaged within layers and across all animals. The ROI is intended to cover a bit more than GM, only. The closest CSF and WM are also included to see how the signal goes to baseline without partial voluming. Standard errors across subjects are shown. The baseline $CBV_{rest}$ is strongly dominated from the superficial layers (black arrow) reflecting known vascular size/density. As indicated in panel A), VASO and MION profile in their native units of % volume change, diverge at the superficial cortical layers (pink arrow). **Panel C)** shows that when the same data are evaluated in the same physical units of absolute ΔCBV (ml / 100 ml of tissue), an additional signal component in the superficial layers becomes apparent in the MION data. While the quantitative ΔCBV (ml / 100 ml of tissue) in VASO is estimated by means of percent signal change, the quantitative ΔCBV (ml / 100 ml of tissue) in MION is estimated by means of the exponential equation (Eq. (6)). Only when VASO and MION based fMRI signals are analysed with the same physical units, the resulting layer-fMRI profiles are comparable. The superficial shaded band in purple is referring to layer IV, which is expected to receive much of the thalamic input during stimulation. Note also that the resolution used here is not sufficient to Nyquist-sample all individual cortical layers separately. Instead, each data point of each cortical depth in the depicted profile refers to a signal mixture with relative partial voluming of neighbouring cortical 'layers'. The cortical depth is given (as a relative fraction of 2 mm) on the x-axis. The position of GM/CSF and GM/WM borders and all relative depth in between are associated with the minimal resolution of the voxel size (0.47 mm). Note that unlike in the OIS-VASO comparisons, the VASO data presented here are shown in absolute CBV changes and have not been normalised by assuming literature values of $CBV_{rest}$. (For interpretation of the references to colour in this figure legend, the reader is referred to the web version of this article.)

blood volume change per 100 ml of tissue) the CBV cortical depth resolved responses between VASO and MION fMRI are in agreement.

When analyzed in the same physical units (ml blood volume change per 100 ml of tissue) the CBV response in the superficial layers becomes indistinguishable between VASO and MION fMRI. Panel C in Fig. 4 depicts the MION and VASO layer profiles in the same physical units. In order to estimate MION CBV profile from signal changes (in MR units) to absolute CBV changes, we used the quantitative Eq. (6). The occurrence of multiple layer peaks can be indicative of thalamic input into multiple layers as suggested in (Constantinople and Bruno, 2013; Harris et al., 2019), and from stimulus induced feedback via corticocortical connections.

### 3.3. Cross species comparison

Since VASO is a non-invasive contrast, and the resulting CBV measures show improved spatial localisation, with proven little venous weighting compared to BOLD fMRI, it is ideally suited for translational neuroimaging. The VASO approach used here, with the same sequence parameters across species (rat and human), opens up new potential translation of research findings from the preclinical settings to human neuroscience (cognitive research based) for laminar based brain studies. Unfortunately, animal and human research on functional brain mapping to this day remains in separate silos with limited cross-over. Interpretation of human fMR imaging data in terms of neuronal inputs and layer projections would benefit from animal studies in which VASO and electrophysiology could be completed concurrently (Logothetis et al., 2001). While VASO may help converge the fields of study, we do of course recognise that there are obvious anaesthetic confounds here, but this is at least a step in the right direction.

Figure 5 depicts cortical profiles of VASO and BOLD fMRI responses for stimulation in the primary somatosensory cortex (whiskers for rats and fingers for humans) (Arkley, 2014; Arkley et al., 2014). The qualitative shapes of the profiles are very similar. In both species, BOLD shows the strongest response toward the cortical surface, while VASO shows strongest activation changes within GM. Note that the nominal resolution of the rat results (0.47 mm) is almost double the resolution of the human results (0.75 mm). The biggest qualitative difference across species is that the bimodal layer response is better visible in rats compared to humans. This is most likely due to the increase partial voluming with the larger voxel sizes in humans. Note that the somatosensory stimulation task across panels A and B, however, was different. While rats were electrically stimulated in the whisker area, humans passively stroked with a abrasive cushion.

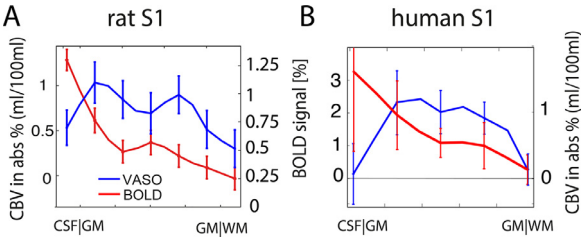


**Fig. 5. Cortical profiles of BOLD and VASO signal change in rat S1 (A) and human S1 (B).** Data shown refer to averages across five rats and nine human participants, respectively. Laminar-dependent profiles reveal different shapes for VASO and BOLD fMRI. BOLD signal change is highly dominated from surface laminae (resulting from known vascular weighting), while VASO peaks in middle cortical laminae, presumably reflecting thalamocortical input, as expected. Note the different scaling of the y-axis in panel A) and B). Error bars refer to standard error of mean across participants. Note also that the resolution used here is not sufficient to Nyquist-sample all individual cortical layers separately. Instead, each data point of each cortical depth in the depicted profile refers to a signal mixture with relative partial voluming of neighbouring layers. This is particularly relevant for human data that are acquired with partial Fourier factor 6/8 and might suffer from more signal blurring.

In order to relate the observed signal responses of passive touch with more established active finger tapping tasks of previous literature, we investigated the influence of active and passive somatosensory stimulations on the magnitude of CBV changes. Thus, experiments were repeated in humans with additional active and passive (sensory only) somatosensory stimulation tasks. We measured the CBV response to brushing and piezo-electric vibrations to achieve this. Fig. 6 depicts the respective CBV activation maps and the corresponding group averages of the layer-depend CBV profiles. It can be seen that passive somatosensory stimulation (brushing and piezo) results in 3–4 times smaller CBV responses compared to active finger tapping (similar results are found for respiratory challenge - see Fig. 3C). The magnitude of passive stimulation-induced CBV change in humans is comparable to the response magnitude in rats (horizontal black line in panel C of Fig. 6).

## 4. Discussion

In this study, we compared high-resolution functional brain imaging modalities in the primary somatosensory cortex in both humans and rats. We used these comparisons to validate that the popular VASO contrast is indeed independent of unwanted signals from large drain-

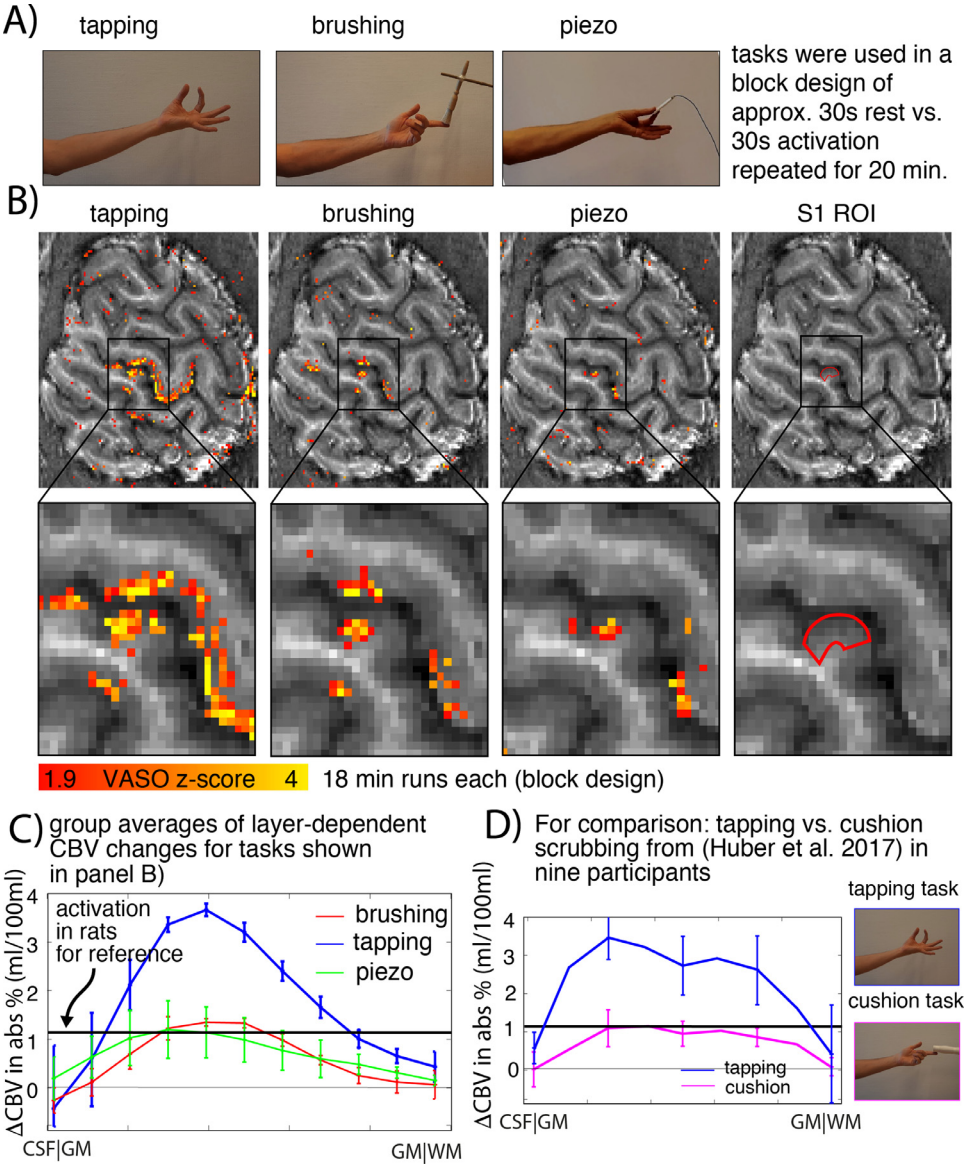


**Fig. 6. Layer-dependent CBV results for various somato-sensory stimulation paradigms.** Data exemplifies that tapping induced activation changes in the primary somatosensory stimulation are significantly stronger than tasks that do not include active movement. This suggests that the different CBV response magnitude between existing rat and human data (often used as evidence to discredit VASO contrast/signal source understanding) is due to the use of active vs. passive sensory tasks. **Panel A)** depicts the different tasks that are used here to induce activation in the primary somatosensory cortex: active pinch-like finger movement of thumb and index finger, passive brushing of the index finger with a non-metal brush, vibration of the thumb and index finger with a piezo-electric device, and a passive touch with an abrasive cushion (replicated from a previous study (Huber et al., 2019)). **Panel B)** depicts activation maps of CBV change of a single representative participant. It can be seen that in the index finger region of the primary somatosensory cortex (highlighted in red), the task-induced CBV change is largest for tapping induced activation. **Panel C)** depicts the corresponding group-averaged layer profiles. While all of the tasks show similar layer-profiles that peak within GM, the overall magnitude is highly variable across tasks. The tapping induced (active) activation is 3–4 times stronger than tasks that are passive sensory trials. **Panel D)** depicts corresponding results from a previous study (Huber et al., 2019) using a slightly different touching task, with the same conclusion. It is noted that the shape of the profile is highly affected by the effective spatial resolution and corresponding partial voluming effects. (For interpretation of the references to colour in this figure legend, the reader is referred to the web version of this article.)

ing veins. This higher localization specificity of CBV-based methods has been expected from previous preclinical work with c-Fos expression (Lu et al., 2004b) and comparison studies of MION CBV and electrophysiology (Poplawsky et al., 2015). This study underscores VASO's usability for layer-fMRI application studies in humans.

### 4.1. Validation of CBV weighting in VASO

Previous VASO validation studies in humans have used contrast agent-based methods; including Gd DTPA (Lin et al., 2011), MION (Jin and Kim, 2008) and PET-tracers (Uh et al., 2011). CBV-weighting was qualitatively compared by averaging low spatial resolution data across large ROIs covering the whole visual cortex. Following this unrefined approach, VASO signal was found to be qualitatively comparable to CBV changes measured with Gd DTPA across different stimulation frequencies (Lin et al., 2011); but offered little in terms of cortical depth profiling.

In preclinical models, Jin and Kim (2006, 2008) implemented a version of VASO for ultra high resolution fMRI. Their VASO method provided reliable CBV weighting in deep cortical layers, where CBF macrovasculature effects and BOLD contaminations are minimized. Here, upon explicit exclusion of signal from inflow-contaminated superficial cortical layers, VASO activation patterns were found to be similar compared to results from iron oxide contrast agent based fMRI signals. The work by Jin and Kim represents the first comparison of VASO and MION results across cortical depth and builds the basis for the follow-up validations shown in Fig. 4.

In contrast with the initial VASO studies more than a decade ago, the results shown in the present study are acquired with an adapted VASO method that can account for i) unwanted inflow flow effects in superficial cortical layers and ii) confounding BOLD contamination. Hence, the presented results in this study enable the first quantitative spatio-temporal validation of VASO across cortical depths. Data shown in Figs. 2, 3 and 5 validate the CBV weighting of VASO in reference to the spatial sensitivity of large draining veins and with respect to temporal features such as a slow post-stimulus recurrence to baseline. Furthermore, whole-region VASO-CBV and OIS-HbT measures in response to both neuronal activation and respiratory challenge are of the same magnitude (within error) in terms of their respective quantitative changes (volume fraction vs. hematocrit).

### 4.2. Differences between rats and humans

The experimental methods (OIS and fMRI) and setups applied across species (OIS and fMRI in rats and fMRI in humans) are quite different in many aspects and rely on various different assumptions. These differences across methods may be impacting the results discussed in this section.

Since VASO is a non-invasive method for CBV mapping, localised to the active brain region and displaying limited macro-vessel weighting, it offers a unique chance for translation between preclinical research and human neuroscience. VASO fMRI allows researchers to compare estimates of CBV cortical layers between humans and animal models by means of the same easily implemented imaging modality. As such, often used arguments citing discrepancies between human and preclinical results can no longer be attributed to the use of different imaging modalities (e.g. MION vs. VASO). Instead, any remaining discrepancies between human and preclinical results in humans and preclinical models can instead be attributed to the important real differences in vascular or neuronal physiology and function. For example, the results shown in Figs. 3C and 5 suggest significantly stronger CBV changes in the primary somatosensory cortex in humans as compared to rats. Such differences are well documented in the literature (Kim and Ogawa, 2012). Due to lack of further comparative inter-species data, it was previously suggested that such discrepancies are a result of different imaging modalities, rather than inter-species differences or anesthesia effects (van Zijl et al., 2012); and in some cases such differential findings were used to question the actual signal source of the SS-SI-VASO approach. Here we compared the functional signal magnitude across a wide spectrum of somatosensory stimulation tasks in humans. Common touch tasks are active processes instigated by the participant themselves and therefore, it can be hypothesized, triggering higher-order functions (reading instructions, paying attention to the screen, eliciting a motor task to generate sensory sensation - finger tapping). Somatosensory stimulation in anesthetized rats is entirely passive. In this in-depth study we explored a similarly passive touch stimulus in human participants, providing evidence that different activation strengths are largely due to the specific somatosensory task (either active tapping or passive touch). While finger movement-induced CBV changes in the primary sensory cortex resulted in 3–4 times larger VASO responses compared to rats, a similar passive sensory-only task gave VASO response magnitudes that were identical (within error) across species.

In this study, we compare human results obtained in the hand area of the primary somatosensory cortex with rat results in the whisker barrel cortex. While it can be argued that we are therefore investigating different touch sensors and the data are incomparable, we emphasize that the areas chosen, hand/fingers & whisker, are responsible for neural processing of the primary form of active touch in both species, respectively. Thus, while we expect interspecies differences of the size and role of superficial layer II (Hill and Walsh, 2005), these brain systems are among the most suitable brain systems for interspecies comparisons (Arkley, 2014; Arkley et al., 2014). Note however, that there might be residual sources of variance across the two compared experimental settings with respect to the size of the engaged stimulated body part. As such, we previously showed that a stimulation of the whole barrel stimulation (as done in this study), evokes a three to four times larger vascular response compared to single whisker stimulation (Berwick et al., 2008). The small optical imaging derived heamodynamic changes observed to single whisker stimulation rule it out as a model for fMRI use (BOLD/CBV signals induced would be too small to detect over current noise limits). In the present study we used a single digit stimulation in humans, while we used a whole whisker pad stimulation in rats in order to match the area of the engaged cortex to be $\approx$ 1–3 mm in diameter. However, more research is needed to rule out further potential sources of task effects across the experimental setup.

The stimulation design in the rat experiments was optimized to be minimally affected by the anesthesia protocol. Namely, in a preparatory study, we found that the hemodynamic response to a 5 Hz stimulation frequency was almost identical (indistinguishable within error) between awake and anesthetized rats (see Fig. 7 in Martin et al. (2006)). Thus, we believe that the anesthesia state is only introducing minor sources of inter species variance. Though, further research is needed to quantify anesthesia effects in this setup across different compartments of the vascular tree.

### 4.3. VASO-MION comparisons across cortical depth

When analysed in relative percent signal changes of $(S_{act} - S_{rest})/S_{rest}$ (as in Eq. (7)), the CBV-weighted layer profiles show some deviation at the cortical surface (Fig. 4c). This surprising difference could be due to a subtle difference in the contrast generation of VASO and MION fMRI. While VASO is a $T_1$-weighted contrast, whose signal is linearly proportional to the voxel's CBV change, MION is a $T_2^*$-weighted contrast that has an exponential dependency to the voxel's CBV change. The subtle difference in these two contrast mechanisms becomes apparent in voxels of very short $T^*_{2\,post-injection} << TE$ and can introduce some differences compared to VASO. These differences will be amplified by the long echo times and voxels with short $T_2^*$ (e.g. due to relatively large MION concentration). However, when analysed by means of the non-linear signal model in Eq. (6), MION and VASO provide the same results (both cortical profile shape and magnitude) within error.

While this non-linear (exponential) signal model was necessary in the study described here, it has not been necessary in previous studies. As such, for experiments where the assumption $\Delta R_2^* << TE$ holds, (i.e., in cases with low contrast dosage, low $CBV_{rest}$, low field strengths, long TEs), the decay in Eq. (2) becomes approximately linear and thus the MION percent signal change in this case would be approximately proportional to $\Delta CBV$, directly representing the VASO responses.

### 4.4. Physical units of CBV change in VASO-OIS comparisons

Unlike MION MRI, OIS does not provide estimates about the baseline CBV. OIS provides estimates of CBV change in relative percent units. Thus, it was not straightforwardly possible to compare VASO with OIS results in VASO's native units of Δml per 100 ml of tissue. For this reason, using the large body of VASO literature, we converted the raw quantitative VASO signal change into relative ΔCBV changes by means of normalizing it to an assumed value of $CBV_{rest}$ (Donahue et al., 2006; Gu et al., 2006; Hua et al., 2009; Huber et al., 2014b; Jin and Kim, 2008; Lu et al., 2003; 2013; 2004b; 2004c; Poser and Norris, 2007; Scouten and Constable, 2007; 2008; Shen et al., 2009; Uh et al., 2011; Wu et al., 2010). Consistently with these earlier VASO studies, a value of $CBV_{rest}$ = 5.5% was assumed. Even though the corresponding VASO-$\Delta CBV$ results are within error to OIS-ΔHbT results, for a slightly larger value of $CBV_{rest}$ = 6.5%, the quantitative estimates of VASO-ΔCBV and OIS-ΔHbT results would be identical (see green best fit line in Fig. 3). Newer evidence suggests such large $CBV_{rest}$ values in rats (Gharagouzloo et al., 2017). The result that an optimal correspondence between VASO CBV and OIS HbT would be found for slightly larger assumed values of $CBV_{rest}$ might be related to the fact that the OIS is mostly sensitive to superficial cortical layers, which have a higher vascular density than deeper layers and are thus above the assumed 5.5% value (see Fig. 4B).

### 4.5. Size of stimulus induced CBV changes

In this study, we report CBV changes in the order of 3.5 ml per 100 ml of tissue for active movement tasks in humans and about 1 ml per 100 ml of tissue for passive somatosensory tasks in animals (and humans). A 3.5 ml CBV change per 100 ml of tissue for strong active tasks is in good agreement with previous VASO-CBV studies at laminar resolutions (Beckett et al., 2020; Goense et al., 2012; Guidi et al., 2020; Huber et al., 2017, 2020). However, dependent on the assumed baseline CBV and the assumed CBV-CBF coupling, a human CBV increase of 3.5 ml per 100 ml of tissue appears surprisingly large in comparison to the results of other CBV based methods. Previous gadolinium-based CBV studies at 4 mm resolutions in humans demonstrated a CBV increase of 1.5 ml per 100 ml of tissue (Uh et al., 2011).

Data from the present study addresses this scepticism directly. The SS-SI-VASO signal source was validated through multimodal imaging (with established fMRI and optical based CBV methods) in animal models. We have shown that for passive stimulation of the whisker pad CBV changes measured with optical, contrast based and VASO are in very good agreement. This data validates the contrast origin of VASO and shows we are sensitive to absolute CBV changes. We use the same VASO pulse sequence in our animal and human studies. Therefore one can conclude that the sequence provides similarly reliable results for stronger tasks in different species. Thus, the large 3.5 ml/100ml tissue CBV changes measured in our human participants are indeed realistic. We therefore hypothesise that the previously reported smaller values (≈ 1.5 ml/100ml tissue) of CBV changes measured with a gadolinium contrast agent is simply a result of partial volume effects. In fact, the study by Uh et al. (2011) also performed VASO experiments at the same resolution and reported almost identical values. In comparable studies of BOLD and CBF, it is reported that larger activation scores for smaller voxels, compared to larger voxels, is solely due to partial voluming (Pfeuffer et al., 2002; Stelzer et al., 2014). Note that dependent upon the CBV units used to quantify CBV change in VASO, underestimation of assumed baseline CBV values can make the relative CBV changes appear unrealistically high. For further discussion the reader is referred to: https://layerfmri.com/cbvbaseline/.

### 4.6. The application of VASO beyond the purpose of contrast validation

In this study, the experimental setup was designed for the purpose of validating the signal origin of VASO with strong block-designed tasks and primary somatosensory areas. For applications of layer-fMRI VASO across a wide range of brain areas see the review article by Finn et al. (2020), for the challenges with event related designs and how to overcome them see Yu et al. (2019), and for sub-second TR layer-fMRI VASO uncovering fast temporal events see the MAGEC VASO approach in Huber et al. (2020a). Although overall contrast to noise for SS-SI-VASO is lower than BOLD equivalents, by overcoming such challenges and validating the signal source of the VASO contrast here, we strengthen the reliability of VASO for layer-fMRI CBV measures. This helps meet the constant push to find functional imaging markers more closely related to neuronal activity and not confounded by blood oxygenation.

Note that even though functional CBV mapping has the advantages of insensitivity to large draining veins and quantification estimated in meaningful physical units that allow better comparison across brain areas and participants, this does not mean that alternative functional contrasts lack advantages. In fact, most neuroscientific group studies do not rely on a quantifiable contrast, nor are they limited by large draining vein effects. We believe that for neuroscience studies in which neither signal quantification biases nor venous signal bleeding effects are considered to be limiting effects, the larger sensitivity of GE-BOLD or other methods will make them the method of choice.

## 5. Conclusion

We conducted a validation study of layer-dependent VASO fMRI by comparing the SS-SI-VASO MR sequence with established preclinical CBV/HbT imaging modalities (contrast-agent based fMRI and intrinsic optical imaging respectively). We found excellent agreement in terms of both spatial and temporal dynamics between all modalities tested in a rat model. We explored the cortical layer dependency of the CBV responses to somatosensory neuronal activity; comparing preclinical rat data with equivalent data from human participants. When layer-dependent CBV changes are analyzed in the same quantitative physical units, the VASO method provides results that are identical to those obtained from long established preclinical methods based on the infusion of a paramagnetic contrast agent. We found that the resultant CBV response provides better spatial localisation than the equivalent BOLD signal (often weighted by venous macro-vessels), with profile peaks corresponding to individual layer groups of unique cortical pathways. We also found that upon harmonizing the stimulation and using identical hypercapnia breathing challenges across species with the same imaging sequence, the CBV results were stronger in humans compared to animals. This has important consequences for translation of experimental design between preclinical and clinical neuroscience. Finally, this study provides direct evidence that the non-invasive SS-SI-VASO sequence can map CBV quantitatively, and can provide reliable estimates of CBV change at the spatial scale of cortical layers. Indeed with CBV presenting as a more robust correlate of neuronal activity, maintaining signal change even in light of significant physiological changes (which have been demonstrated to dramatically affect BOLD fMRI (Kennerley et al., 2012a)); VASO fMRI should become the method of choice for high resolution layer dependent neuroimaging studies, in which researchers wish to be independent of large draining vein effects and the quantifiability limitations of conventional methods.

## Data and Software availability

The data shown here have been acquired over a period of four years across four institutions with variable data sharing policies. All processed human and rat data are available upon request in anonymized form. Data presented in Fig. 5 are already publicly available from previous publications. Data presented in Fig 6 have been acquired under the York-Maastricht partnership and are available as raw data on Openneuro. We are happy to share the used sequence with the vendor approval for Bruker Paravision (versions 3 to 5), as well as SIEMENS VB17B.

## Credit authorship contribution statement

**Laurentius (Renzo) Huber:** Conceptualization, Methodology, Software, Validation, Formal analysis, Resources, Data curation, Writing – original draft, Writing – review & editing, Supervision, Project administration, Funding acquisition. **Benedikt A Poser:** Conceptualization, Methodology, Software, Validation, Formal analysis, Resources, Data curation, Writing – original draft, Writing – review & editing, Supervision, Project administration, Funding acquisition. **Amanda L Kaas:** Conceptualization, Methodology, Software, Validation, Formal analysis, Resources, Data curation, Writing – original draft, Writing – review & editing, Supervision, Project administration, Funding acquisition. **Elizabeth J Fear:** Conceptualization, Methodology, Software, Validation, Formal analysis, Resources, Data curation, Writing – original draft, Writing – review & editing, Project administration, Funding acquisition. **Sebastian Dresbach:** Conceptualization, Methodology, Software, Validation, Formal analysis, Resources, Data curation, Writing – original draft, Writing – review & editing, Project administration, Funding acquisition. **Jason Berwick:** Conceptualization, Methodology, Software, Validation, Formal analysis, Resources, Data curation, Writing – original draft, Writing – review & editing, Supervision, Project administration, Funding acquisition. **Rainer Goebel:** Conceptualization, Methodology, Software, Validation, Formal analysis, Resources, Data curation, Writing – original draft, Writing – review & editing, Supervision, Project administration, Funding acquisition. **Robert Turner:** Conceptualization, Methodology, Software, Validation, Formal analysis, Resources, Data curation, Writing – original draft, Writing – review & editing, Supervision, Project administration, Funding acquisition. **Aneurin J Kennerley:** Conceptualization, Methodology, Software, Validation, Formal analysis, Resources, Data curation, Writing – original draft, Writing – review & editing, Supervision, Project administration, Funding acquisition..

## Acknowledgements

**Data interpretation**: We thank, Martin Havlicek, Natalia Petridou, Kamil Uludag, and Ben Inglis for discussions about the expected baseline CBV.

**Animal Husbandry**: We thank the technical team within the biological services unit at the University of Sheffield for animal husbandry support.

**Data Acquisition**: We thank Kenny Chung for radiographic assistance with experiments conducted at NIH. We thank FMRIF (especially Sean Marrett), and Scannexus (especially Chris Wiggins), where MBIC data were acquired. We thank Dimo Ivanov for the setup of the Hypercapnia delivery system used for the experiments in humans.

**Safety supervision of human experiments**: We thank Dr. Ilona Henseler, Dr. Elisabeth Roggenhofer, and Dr. Stephan Kabisch for medical supervision of experiments with hypercapnia. We thank Chris Wiggins, and Bianca Linssen for help with the safe application of human finger brushing inside the scanner bore.

**Financial interest**: Rainer Goebel works for Brain Innovation and has financial interests tied to the company.

## Funding

Renzo Huber and Aneurin J Kennerley received funding from the York-Maastricht partnership for this project. Renzo Huber was funded from the NWO VENI project 016.Veni.198.032 for part of the study. Benedikt Poser is partially funded by the NWO VIDI grant 16.Vidi.178.052 and by the National Institute for Health grant (R01MH/111444) (PI David Feinberg). Rainer Goebel has received funding from the European Union's Horizon 2020 Framework Programme for Research and Innovation under the Specific Grant Agreement No. 945539 (Human Brain Project SGA3). The preclinical studies presented here were supported by a United Kingdom Medical Research Council (MRC) grant MR/M013553/1 and Wellcome Trust (WT) Grant 093069/Z/10/Z. Sebastian Dresbach is supported by the 'Robin Hood' fund of the Faculty of Psychology and Neuroscience and the department of Cognitive Neuroscience. We thank Harald E Möller and the NMR-group of the MPI-CBS for supporting the part of this study that was conducted at the MPI in Leipzig. Parts of the human fMRI data were acquired with the great support of Scannexus BV, Maastricht, NL (www.scannexus.nl).

## References

Arkley, K., 2014. Rats use their whiskers in a similar way to how humans use their hands and fingers. ScienceDaily 1. https://www.sciencedaily.com/releases/2014/07/140707141652.htm

Arkley, K., Grant, R.A., Mitchinson, B., Prescott, T.J., et al., 2014. Strategy change in vibrissal active sensing during rat locomotion. Curr. Biol. 24 (13), 1507–1512. doi:10.1016/j.cub.2014.05.036.

Assaf, Y., 2019. Imaging laminar structures in the gray matter with diffusion MRI. Neuroimage 197 (December 2017), 677–688. doi:10.1016/j.neuroimage.2017.12.096.

Attwell, D., Iadecola, C., 2002. The neural basis of functional brain imaging signals. Trends Neurosci. 25 (12), 621–625. doi:10.1016/S0166-2236(02)02264-6.

Beckett, A.J.S.S., Dadakova, T., Townsend, J., Huber, L., Park, S., Feinberg, D.A., et al., 2020. Comparison of BOLD and CBV using 3D EPI and 3D GRASE for cortical layer fMRI at 7T. Magn. Reson. Med. 1–18. doi:10.1101/778142.

Berwick, J., Johnston, D., Jones, M., Martindale, J., Martin, C., Kennerley, A.J., Redgrave, P., Mayhew, J.E.W., et al., 2008. Fine detail of neurovascular coupling revealed by spatiotemporal analysis of the hemodynamic response to single whisker stimulation in rat barrel cortex. J. Neurophysiol. 99 (2), 787–798. doi:10.1152/jn.00658.2007.

Berwick, J., Martin, C., Martindale, J., Jones, M., Johnston, D., Zheng, Y., Redgrave, P., Mayhew, J., et al., 2002. Hemodynamic response in the unanesthetized rat: intrinsic optical imaging and spectroscopy of the barrel cortex. J. Cereb. Blood Flow Metab. 22 (6), 670–679. doi:10.1097/00004647-200206000-00005.

Brodmann, K., 1909. Vergleichende Lokalisationslehre der Großhirnrinde. Johann Ambrosius Barth. papers3://publication/uuid/E388F0E9-1C79-49C1-94B1-F8730252C625

Calamante, F., Thomas, D.L., Pell, G.S., Wiersma, J., Turner, R., et al., 1999. Measuring cerebral blood flow using magnetic resonance imaging techniques. J. Cereb. Blood Flow Metab. 19 (7), 701–735. http://ovidsp.ovid.com/ovidweb.cgi?T=JS&PAGE=reference&D=emed4&NEWS=N&AN=2000107356

Chai, Y., Li, L., Huber, L., Poser, B.A., Bandettini, P.A., et al., 2019. Integrated VASO and perfusion contrast: a new tool for laminar functional MRI. Neuroimage 116358. doi:10.1016/j.neuroimage.2019.116358.

Chance, B., 1991. Optical method. Annu. Rev. Biophys. Biophys. Chem 20, 1–28. doi:10.1146/annurev.biochem.64.1.721.

Chu, K.C., Xu, Y., Balschi, J.A., Springer, C.S., et al., 1990. Bulk magnetic susceptibility shifts in nmr studies of compartmentalized samples: use of paramagnetic reagents. Magn Reson Med 13 (2), 239–262. doi:10.1002/mrm.1910130207.

Constantinople, C.M., Bruno, R.M., 2013. Deep cortical layers are activated directly by Thalamus. Science 1591 (June), 1591–1594. doi:10.1126/science.1236425.

Cox, R., 1996. AFNI: software for analysis and visualization of functional magnetic resonance neuroimages. Comput. Biomed. Res. 29 (29), 162–173. doi:10.1006/cbmr.1996.0014.

Donahue, M.J., Hua, J., Pekar, J.J., Van Zijl, P.C.M., et al., 2009. Effect of inflow of fresh blood on vascular-space-occupancy (VASO) contrast. Magn. Reson. Med. 61 (2), 473–480. doi:10.1002/mrm.21804.

Donahue, M.J., Juttukonda, M.R., Watchmaker, J.M., 2017. Noise concerns and post-processing procedures in cerebral blood flow (CBF) and cerebral blood volume (CBV) functional magnetic resonance imaging. Neuroimage 154, 43–58. doi:10.1016/j.neuroimage.2016.09.007.

Donahue, M.J., Lu, H., Jones, C.K., Edden, R.A.E., Pekar, J.J., Van Zijl, P.C.M., et al., 2006. Theoretical and experimental investigation of the VASO contrast mechanism. Magn. Reson. Med. 56 (6), 1261–1273. doi:10.1002/mrm.21072.

Douglas, R.J., Martin, K.A.C., 2004. Neuronal circuits of the neocortex. Annu. Rev. Neurosci. 27 (1), 419–451. doi:10.1146/annurev.neuro.27.070203.144152.

Douglas, R.J., Martin, K.A.C., 2004. Neuronal circuits of the neocortex. Annu. Rev. Neurosci. 27 (1), 419–451. doi:10.1146/annurev.neuro.27.070203.144152.

Duyn, J.H., van Gelderen, P., Li, T.-Q., de Zwart, J.A., Koretsky, A.P., Fukunaga, M., et al., 2007. High-field MRI of brain cortical substructure based on signal phase. Proc. Natl. Acad. Sci. 104 (28), 11796–11801. doi:10.1073/pnas.0610821104.

Economo, C., Koskinas, G.N., 1925. Die cytoarchitektonik der hirnrinde des erwachsenen menschen. J. Anat. 61, 264–266.
Eickhoff, S., Walters, N.B., Schleicher, A., Kril, J., Egan, G.F., Zilles, K., Watson, J.D.G., Amunts, K., et al., 2005. High-resolution MRI reflects myeloarchitecture and cytoarchitecture of human cerebral cortex. Hum. Brain Mapp. 24 (3), 206–215. doi:10.1002/hbm.20082.
Feinberg, D.A., Harel, N., Ramanna, S., Uğurbil, K., Yacoub, E., et al., 2008. Sub-millimeter single-shot 3D GRASE with inner volume selection for T2 weighted fMRI applications at 7 Tesla 1. Proc. Intl. Soc. Mag. Reson. Med. 16 37 (4), 2373.
Finn, E.S., Huber, L., Bandettini, P.A., 2020. Higher and deeper: bringing layer fMRI to association cortex. Prog. Neurobiol. 101930. doi:10.1016/j.pneurobio.2020.101930.
Finn, E.S., Huber, L., Jangraw, D.C., Molfese, P.J., Bandettini, P.A., et al., 2019. Layer-dependent activity in human prefrontal cortex during working memory. Nat. Neurosci. 22, 1687–1695. doi:10.1038/s41593-019-0487-z.
Fracasso, A., Luijten, P.R., Dumoulin, S.O., Petridou, N., et al., 2018. Laminar imaging of positive and negative BOLD in human visual cortex at 7 T. Neuroimage 164 (February), 100–111. doi:10.1016/j.neuroimage.2017.02.038.
Gagnon, L., Sakadzic, S., Lesage, F., Musacchia, J.J., Lefebvre, J., Fang, Q., Yücel, M.A., Evans, K.C., Mandeville, E.T., Cohen-Adad, J., Polimeni, J.R., Yaseen, M.A., Lo, E.H., Greve, D.N., Buxton, R.B., Dale, A.M., Devor, A., et al., 2015. Quantifying the microvascular origin of BOLD-fMRI from first principles with two-photon microscopy and an oxygen-sensitive nanoprobe. J. Neurosci. 8 (3–4), 307–310. doi:10.1523/JNEUROSCI.3555-14.2015.
Gharagouzloo, C.A., Timms, L., Qiao, J., Fang, Z., Nneji, J., Pandya, A., Kulkarni, P., van de Ven, A.L., Ferris, C., Sridhar, S., et al., 2017. Quantitative vascular neuroimaging of the rat brain using superparamagnetic nanoparticles: new insights on vascular organization and brain function. Neuroimage 163 (September), 24–33. doi:10.1016/j.neuroimage.2017.09.003.
Goa, P.E., Koopmans, P.J., Poser, B.A., Barth, M., Norris, D.G., et al., 2014. Bold fMRI signal characteristics of S1- and S2-SSFP at 7 Tesla. Front. Neurosci. 8 (8 MAR), 1–7. doi:10.3389/fnins.2014.00049.
Goense, J.B.M., Merkle, H., Logothetis, N.K., 2012. High-Resolution fMRI reveals laminar differences in neurovascular coupling between positive and negative BOLD responses. Neuron 76 (3), 629–639. doi:10.1016/j.neuron.2012.09.019. http://www.sciencedirect.com/science/article/pii/S0896627312008549
Goense, J.B.M., Zappe, A.C., Logothetis, N.K., 2007. High-resolution fMRI of macaque V1. Magn. Reson. Imaging 25 (6), 740–747. doi:10.1016/j.mri.2007.02.013.
Gray, L.H., Steadman, J.M., 1964. Determination of the oxyhaemoglobin dissociation curves for mouse and rat blood. J. Physiol. 175 (2), 161–171. doi:10.1113/jphysiol.1964.sp007509.
Gu, H., Lu, H., Ye, F.Q., Stein, E.A., Yang, Y., et al., 2006. Noninvasive quantification of cerebral blood volume in humans during functional activation. Neuroimage 30 (2), 377–387. doi:10.1016/j.neuroimage.2005.09.057.
Guidi, M., Huber, L., Lampe, L., Gauthier, C.J., Möller, H.E., et al., 2016. Lamina-dependent calibrated BOLD response in human primary motor cortex. Neuroimage 141, 250–261. doi:10.1016/j.neuroimage.2016.06.030.
Guidi, M., Huber, L., Lampe, L., Merola, A., Ihle, K., Möller, H.E., et al., 2020. Cortical laminar resting-state fluctuations scale with the hypercapnic bold response. Hum. Brain Mapp 41, 2014–2027. doi:10.1002/hbm.24926.
Harris, J.A., Mihalas, S., Hirokawa, K.E., Whitesell, J.D., Choi, H., Bernard, A., Bohn, P., Caldejon, S., Casal, L., Cho, A., Feiner, A., Feng, D., Gaudreault, N., Gerfen, C.R., Graddis, N., Groblewski, P.A., Henry, A.M., Ho, A., Howard, R., Knox, J.E., Kuan, L., Kuang, X., Lecoq, J., Lesnar, P., Li, Y., Luviano, J., McConoughey, S., Mortrud, M.T., Naeemi, M., Ng, L., Oh, S.W., Ouellette, B., Shen, E., Sorensen, S.A., Wakeman, W., Wang, Q., Wang, Y., Williford, A., Phillips, J.W., Jones, A.R., Koch, C., Zeng, H., et al., 2019. Hierarchical organization of cortical and thalamic connectivity. Nature 575 (7781), 195–202. doi:10.1038/s41586-019-1716-z.
Hill, R.S., Walsh, C.A., 2005. Molecular insights into human brain evolution. Nature 437 (7055), 64–67. doi:10.1038/nature04103.
Hillman, E.M.C., Devor, A., Bouchard, M.B., Dunn, A.K., Krauss, G.W., Skoch, J., Bacskai, B.J., Dale, A.M., Boas, D.A., et al., 2007. Depth-resolved optical imaging and microscopy of vascular compartment dynamics during somatosensory stimulation. Neuroimage 35 (1), 89–104. doi:10.1016/j.neuroimage.2006.11.032.
Hua, J., Donahue, M.J., Zhao, J.M., Grgac, K., Huang, A.J., Zhou, J., Van Zijl, P.C.M., et al., 2009. Magnetization transfer enhanced vascular-space-occupancy (MT-VASO) functional MRI. Magn. Reson. Med. 61 (4), 944–951. doi:10.1002/mrm.21911.
Hua, J., Jones, C.K., Qin, Q., Van Zijl, P.C.M., et al., 2013. Implementation of vascular-space-occupancy MRI at 7T. Magn. Reson. Med. 69 (4), 1003–1013. doi:10.1002/mrm.24334.
Hua, J., Stevens, R.D., Huang, A.J., Pekar, J.J., Van Zijl, P.C.M., et al., 2011. Physiological origin for the BOLD poststimulus undershoot in human brain: vascular compliance versus oxygen metabolism. J. Cereb. Blood Flow Metab. 31 (7), 1599–1611. doi:10.1038/jcbfm.2011.35.
Huber, L., Finn, E.S., Chai, Y., Goebel, R., Stirnberg, R., Marrett, S., Uludag, K., Kim, S.G., Han, S., Bandettini, P.A., Poser, B.A., et al., 2020a. Layer-dependent functional connectivity methods. Prog. Neurobiol.. page in print
Huber, L., Finn, E.S., Handwerker, D.A., Boenstrup, M., Glen, D., Kashyap, S., Ivanov, D., Petridou, N., Marrett, S., Goense, J., Poser, B., Bandettini, P.A., et al., 2020. Sub-millimeter fMRI reveals multiple topographical digit representations that form action maps in human motor cortex. Neuroimage 208, 116463. doi:10.1101/457002.
Huber, L., Goense, J., Kennerley, A.J., Ivanov, D., Krieger, S.N., Lepsien, J., Trampel, R., Turner, R., Möller, H.E., et al., 2014. Investigation of the neurovascular coupling in positive and negative BOLD responses in human brain at 7T. Neuroimage 97, 349–362. doi:10.1016/j.neuroimage.2014.04.022.
Huber, L., Goense, J., Kennerley, A.J., Trampel, R., Guidi, M., Reimer, E., Ivanov, D., Neef, N., Gauthier, C.J., Turner, R., Möller, H.E., et al., 2015. Cortical lamina-dependent blood volume changes in human brain at 7T. Neuroimage 107, 23–33. doi:10.1016/j.neuroimage.2014.11.046.
Huber, L., Handwerker, D.A., Jangraw, D.C., Chen, G., Hall, A., Stüber, C., Gonzalez-Castillo, J., Ivanov, D., Marrett, S., Guidi, M., Goense, J., Poser, B.A., Bandettini, P.A., et al., 2017. High-resolution CBV-fMRI allows mapping of laminar activity and connectivity of cortical input and output in human M1. Neuron 96 (6), 1253–1263.e7. doi:10.1016/j.neuron.2017.11.005.
Huber, L., Ivanov, D., Handwerker, D.A., Marrett, S., Guidi, M., Uludağ, K., Bandettini, P.A., Poser, B.A., et al., 2016. Techniques for blood volume fMRI with VASO: from low-resolution mapping towards sub-millimeter layer-dependent applications. Neuroimage 164 (November), 131–143. doi:10.1016/j.neuroimage.2016.11.039.
Huber, L., Ivanov, D., Krieger, S.N., Streicher, M.N., Mildner, T., Poser, B.A., Möller, H.E., Turner, R., et al., 2014. Slab-selective, BOLD-corrected VASO at 7 Tesla provides measures of cerebral blood volume reactivity with high signal-to-noise ratio. Magn. Reson. Med. 72 (1), 137–148. doi:10.1002/mrm.24916.
Huber, L., Kennerley, A.J., Gauthier, C.J., Krieger, S.N., Maria Guidi, D.I., Turner, R., Möller, H.E., et al., 2014. Cerebral blood volume redistribution during hypercapnia. Imaging Cereb. Physiol. 2, O42. doi:10.7490/f1000research.1115082.1.
Huber, L.R., Poser, B.A., Bandettini, P.A., Arora, K., Wagstyl, K., Cho, S., Goense, J., Nothnagel, N., Morgan, A.T., Van Den Hurk, J., Reynold, R.C., Glen, D.R., Goebel, R.W., Gulban, O.F., et al., 2021. LAYNII: A software suite for layer-fMRI. Neuroimage doi:10.1016/j.neuroimage.2021.118091.
Huber, L., Uludağ, K., Möller, H.E., 2019. Non-BOLD contrast for laminar fMRI in humans: CBF, CBV, and CMRO2. Neuroimage 197, 742–760. doi:10.1016/j.neuroimage.2017.07.041.
Hurley, A.C., Al-Radaideh, A., Bai, L., Aickelin, U., Coxon, R., Glover, P., Gowland, P.A., et al., 2010. Tailored RF pulse for magnetization inversion at ultrahigh field. Magn. Reson. Med. 63 (1), 51–58. doi:10.1002/mrm.22167.
Hutchinson, E.B., Stefanovic, B., Koretsky, A.P., Silva, A.C., et al., 2006. Spatial flow-volume dissociation of the cerebral microcirculatory response to mild hypercapnia. Neuroimage 32 (2), 520–530. doi:10.1016/j.neuroimage.2006.03.033.
Ivanov, D., Poser, B.A., Kashyap, S.S., Gardumi, A., Huber, L., Uludag, K., et al., 2016. Sub-millimeter human brain perfusion imaging using arterial spin labelling at 3 and 7 Tesla. In: Proceedings of the High Field Meeting of the International Society of Magnetic Resonance in Medicine, p. 14.
Ivanov, K.P., Kalinina, M.K., Levkovich, Y.I., 1981. Blood flow velocity in capillaries of brain and muscles and its physiological significance. Microvasc. Res. 22 (2), 143–155.
Jin, T., Kim, S.G., 2006. Spatial dependence of CBV-fMRI: a comparison between VASO and contrast agent based methods. In: Annual International Conference of the IEEE Engineering in Medicine and Biology - Proceedings, 10, pp. 25–28. doi:10.1109/IEMBS.2006.259553.
Jin, T., Kim, S.G., 2008. Improved cortical-layer specificity of vascular space occupancy fMRI with slab inversion relative to spin-echo BOLD at 9.4 T. Neuroimage 40 (1), 59–67. doi:10.1016/j.neuroimage.2007.11.045.
Jin, T., Kim, S.G., 2010. Change of the cerebrospinal fluid volume during brain activation investigated by T1$\rho$-weighted fMRI. Neuroimage 51 (4), 1378–1383. doi:10.1016/j.neuroimage.2010.03.047.
Jones, M., Hewson-Stoate, N., Martindale, J., Redgrave, P., Mayhew, J., et al., 2004. Nonlinear coupling of neural activity and CBF in rodent barrel cortex. Neuroimage 22 (2), 956–965. doi:10.1016/j.neuroimage.2004.02.007.
Kennerley, A.J., Berwick, J., Martindale, J., Johnston, D., Papadakis, N., Mayhew, J.E., et al., 2005. Concurrent fMRI and optical measures for the investigation of the hemodynamic response function. Magn. Reson. Med. 54 (2), 354–365. doi:10.1002/mrm.20511.
Kennerley, A.J., Berwick, J., Martindale, J., Johnston, D., Zheng, Y., Mayhew, J.E., et al., 2009. Refinement of optical imaging spectroscopy algorithms using concurrent BOLD and CBV fMRI. Neuroimage 47 (4), 1608–1619. doi:10.1016/j.neuroimage.2009.05.092.
Kennerley, A.J., Harris, S., Bruyns-Haylett, M., Boorman, L., Zheng, Y., Jones, M., Berwick, J., et al., 2012. Early and late stimulus-evoked cortical hemodynamic responses provide insight into the neurogenic nature of neurovascular coupling. J. Cereb. Blood Flow Metab. 32 (3), 468–480. doi:10.1038/jcbfm.2011.163.
Kennerley, A.J., Huber, L., Mildner, T., Mayhew, J., Turner, R., Möller, H.E., Berwick, J., et al., 2013. Does VASO contrast really allow measurement of CBV at High Field (7T)? An in-vivo quantification using concurrent Optical Imaging Spectroscopy. In: Proc Intl Soc Mag Reson Med, p. 0757. https://cds.ismrm.org/protected/13MProceedings/files/0757.PDF
Kennerley, A.J., Mayhew, J.E., Boorman, L., Zheng, Y., Berwick, J., et al., 2012. Is optical imaging spectroscopy a viable measurement technique for the investigation of the negative BOLD phenomenon? aconcurrent optical imaging spectroscopy and fMRI study at high field (7T). Neuroimage 61 (1), 10–20. doi:10.1016/j.neuroimage.2012.03.015.
Kennerley, A.J., Mayhew, J.E., Redgrave, P., Berwick, J., et al., 2010. Vascular origins of BOLD and CBV fMRI signals: statistical mapping and histological sections compared. Open Neuroimag. J. 4, 1–8. doi:10.2174/1874440001004010001. http://benthamopen.com/ABSTRACT/TONIJ-4-1
Kennerley, A.J., Poser, B.A., Torkelsen, F.H., Goebel, R., Kaas, A., Huber, L., et al., 2020. Cross species validation of the layer-fMRI VASO contrast mechanism: data comparison against pre-clinical 2D-OIS and CBV-MRI gold standards. In: Proc Intl Soc Mag Reson Med, Vol. 22, p. 1103.
Kida, I., Rothman, D.L., Hyder, F., 2007. Dynamics of changes in blood flow, volume, and oxygenation: implications for dynamic functional magnetic resonance imaging calibration. J. Cereb. Blood Flow Metab. 27 (4), 690–696. doi:10.1038/sj.jcbfm.9600409.
Kim, S.-G., Bandettini, P.A., 2010. Principles of Functional MRI. In: Faro, S.H., Mohamed, F.B. (Eds.), BOLD fMRI: A guide to functional imaging for neuroscientists. Springer-Verlag, pp. 3–22. chapter Principles

Kim, S.G., Harel, N., Jin, T., Kim, T., Lee, P., Zhao, F., et al., 2013. Cerebral blood volume MRI with intravascular superparamagnetic iron oxide nanoparticles. NMR Biomed. 26 (8), 949–962. doi:10.1002/nbm.2885.

Kim, S.G., Ogawa, S., 2012. Biophysical and physiological origins of blood oxygenation level-dependent fMRI signals. J. Cereb. Blood Flow Metab. 32 (7), 1188–1206. doi:10.1038/jcbfm.2012.23.

Kim, S.G., Ugurbil, K., 2003. High-resolution functional magnetic resonance imaging of the animal brain. Methods 30 (1), 28–41. doi:10.1016/S1046-2023(03)00005-7.

Kim, T., Hendrich, K.S., Masamoto, K., Kim, S.G., et al., 2007. Arterial versus total blood volume changes during neural activity-induced cerebral blood flow change: implication for BOLD fMRI. J. Cereb. Blood Flow Metab. 27 (6), 1235–1247. doi:10.1038/sj.jcbfm.9600429.

Kleinfeld, D., Mitra, P.P., Helmchen, F., Denk, W., et al., 1998. Fluctuations and stimulus-induced changes in blood flow observed in individual capillaries in layers 2 through 4 of rat neocortex. Proc. Natl. Acad. Sci. 95 (26), 15741–15746. doi:10.1073/pnas.95.26.15741.

Kong, Y., Zheng, Y., Johnston, D., Martindale, J., Jones, M., Billings, S., Mayhew, J., et al., 2004. A model of the dynamic relationship between blood flow and volume changes during brain activation. J. Cereb. Blood Flow Metab. 24 (12), 1382–1392. doi:10.1097/01.WCB.0000141500.74439.53.

Kurban, D., Huber, L., Liberman, G., Kashyap, S., Ivanov, D., Poser, B.A., et al., 2020. Making fMRI sequences more efficient: combining SMS spiral readout with blood volume-sensitive VASO. Proc. Organ. Hum. Brain Mapp. 26, 1534.

Larkum, M.E., Petro, L.S., Sachdev, R.N.S., Muckli, L., et al., 2018. A perspective on cortical layering and layer-spanning neuronal elements. Front. Neuroanat. 12 (July), 1–9. doi:10.3389/fnana.2018.00056.

Lashley, K.S., Clark, G., 1946. The cytoarchitecture of the cerebral cortex of ateles: a critical examination of architectonic studies. J. Comp. Neurol. 85 (2), 223–305. doi:10.1002/cne.900850207.

Lee, S.P., Duong, T.Q., Yang, G., Iadecola, C., Kim, S.G., et al., 2001. Relative changes of cerebral arterial and venous blood volumes during increased cerebral blood flow: implications for bold fMRI. Magn. Reson. Med. 45 (5), 791–800. doi:10.1002/mrm.1107.

Leuze, C.W.U., Anwander, A., Bazin, P.-L., Dhital, B., Stüber, C., Reimann, K., Geyer, S., Turner, R., 2014. Layer-specific intracortical connectivity revealed with diffusion MRI. Cereb. Cortex 24 (2), 328–339. doi:10.1093/cercor/bhs311. https://academic.oup.com/cercor/article-lookup/doi/10.1093/cercor/bhs311

Lieke, E.E., Frostig, R.D., Arieli, A., Ts'o, D.Y., Hildesheim, R., Grinvald, A., et al., 1989. OPTICAL IMAGING OF CORTICAL imaging based on slow intrinsic-signals. Annu. Rev. Physiol 51, 543–559.

Lin, A.-L., Lu, H., Fox, P.T., Duong, T.Q., et al., 2011. Cerebral blood volume measurements: Gd DTPA vs. VASO and their relationship with cerebral blood flow in activated human visual cortex. Open Neuroimaging J. 5, 90–95. doi:10.2174/1874440001105010090. http://www.pubmedcentral.nih.gov/articlerender.fcgi?artid=3245406&tool=pmcentrez&rendertype=abstract

Logothetis, N., Pauls, J., Augath, M., Oeltermann, A., et al., 2001. Neurophysiological investigation of the basis of the fMRI signal what is the exact relationship between the. Nature 412 (6843), 150–157. doi:10.1038/35084005. http://www.ncbi.nlm.nih.gov/pubmed/11449264

Lu, H., 2008. Magnetization "reset" for non-steady-state blood spins in vascular-space-occupancy (VASO) fMRI. In: Proceedings of the 16th Annual Meeting ISMRM, 16, p. 2008. http://cds.ismrm.org/ismrm-2008/files/00406.pdf

Lu, H., Golay, X., Pekar, J.J., Van Zijl, P.C.M., et al., 2004. Sustained poststimulus elevation in cerebral oxygen utilization after vascular recovery. J. Cereb. Blood Flow Metab. 24 (7), 764–770. doi:10.1097/01.WCB.0000124322.60992.5C.

Lu, H., Golay, X., Pekar, J.J., van Zijl, P.C.M., et al., 2003. Functional magnetic resonance imaging based on changes in vascular space occupancy. Magn. Reson. Med. 50, 263–274. doi:10.1002/mrm.10519.

Lu, H., Hua, J., van Zijl, P.C.M., 2013. Noninvasive functional imaging of cerebral blood volume with vascular-space-occupancy (VASO) MRI. NMR Biomed. 26 (8), 932–948. doi:10.1002/nbm.2905.

Lu, H., Law, M., Johnson, G., Ge, Y., Van Zijl, P.C.M., Helpern, J.A., et al., 2005. Novel approach to the measurement of absolute cerebral blood volume using vascular-space-occupancy magnetic resonance imaging. Magn. Reson. Med. 54 (6), 1403–1411. doi:10.1002/mrm.20705.

Lu, H., Patel, S., Luo, F., Li, S.J., Hillard, C.J., Ward, B.D., Hyde, J.S., et al., 2004. Spatial correlations of laminar BOLD and CBV responses to rat whisker stimulation with neuronal activity localized by fos expression. Magn. Reson. Med. 52 (5), 1060–1068. doi:10.1002/mrm.20265.

Lu, H., van Zijl, 2012. A review of the development of vascular-space-occupancy (VASO) fMRI. Neuroimage 62, 736–742. doi:10.1016/j.neuroimage.2012.01.013.

Lu, H., Van Zijl, P.C.M., Hendrikse, J., Golay, X., et al., 2004. Multiple acquisitions with global inversion cycling (MAGIC): a multislice technique for vascular-space-occupancy dependent fMRI. Magn. Reson. Med. 51 (1), 9–15. doi:10.1002/mrm.10659.

Mandeville, J.B., Jenkins, B.G., Kosofsky, B.E., Moskowitz, M.A., Rosen, B.R., Marota, J.J.A., et al., 2001. Regional sensitivity and coupling of BOLD, and CBV changes during stimulation of rat brain. Magn. Reson. Med. 45 (3), 443–447. doi:10.1002/1522-2594(200103)45:3<443::AID-MRM1058>3.0.CO;2-3.

Mandeville, J.B., Marota, J.J.A., Ayata, C., Zaharchuk, G., Moskowitz, M.A., Rosen, B.R., Weisskoff, R.M., et al., 1999. Evidence of a cerebrovascular postarteriole windkessel with delayed compliance. J. Cereb. Blood Flow Metab. 19 (6), 679–689. doi:10.1097/00004647-199906000-00012.

Mandeville, J.B., Marota, J.J.A., Kosofsky, B.E., Keltner, J.R., Weissleder, R., Rosen, B.R., Weisskoff, R.M., et al., 1998. Dynamic functional imaging of relative cerebral blood volume during rat forepaw stimulation. Magn. Reson. Med. 39 (4), 615–624. doi:10.1002/mrm.1910390415.

Martin, C., Martindale, J., Berwick, J., Mayhew, J., et al., 2006. Investigating neural – hemodynamic coupling and the hemodynamic response function in the awake rat. Neuroimage 32, 33–48. doi:10.1016/j.neuroimage.2006.02.021.

Mayhew, J., Zheng, Y., Hou, Y., Vuksanovic, B., Berwick, J., Askew, S., Coffey, P., et al., 1999. Spectroscopic analysis of changes in remitted illumination: the response to increased neural activity in brain. Neuroimage 10 (3 I), 304–326. doi:10.1006/nimg.1999.0460.

Menon, R.S., 2002. Postacquisition suppression of large-vessel BOLD signals in high-resolution fMRI. Magn. Reson. Med. 47 (1), 1–9. doi:10.1002/mrm.10041.

Mispelter, J., Lupu, M., Briguet, A., 2006. NMR Probeheads for Biophysical and Biomedical Experiments: Theoretical Principles & Practical Guidelines. Imperial College Press.

Mortola, J.P., Lanthier, C., et al., 1996. The ventilatory and metabolic response to hypercapnia in newborn mammalian species. Respir. Physiol. 103 (3), 263–270. doi:10.1016/0034-5687(95)00093-3.

Nakai, M., Maeda, M., 1999. Scopolamine-sensitive and resistant components of increase in cerebral cortical blood flow elicited by periaqueductal gray matter of rats. Neurosci. Lett. 270 (3), 173–176. doi:10.1016/S0304-3940(99)00491-7.

Narayanan, R.T., Udvary, D., Oberlaender, M., 2017. Cell type-specific structural organization of the six layers in rat barrel cortex. Front. Neuroanat. 11 (October), 1–10. doi:10.3389/fnana.2017.00091.

Norris, D.G., Polimeni, J.R., 2019. Laminar (f)MRI: a short history and future prospects. Neuroimage 197, 643–649. doi:10.1016/j.neuroimage.2019.04.082.

Oshio, K., Feinberg, D.A., 1991. GRASE (Gradient- and spin-echo) imaging: a novel fast MRI technique. Magn. Reson. Med. 20, 344–349. doi:10.1002/mrm.1910200219.

Pawlik, G., Rackl, A., Bing, R.J., 1981. Quantitative capillary topography and blood flow in the cerebral cortex of cats: an in vivo microscopic study. Brain Res. 208, 35–58. doi:10.1016/0006-8993(81)90619-3.

Penny, W.D., Friston, K.J., Ashburner, J.T., Kiebel, S.J., Nichols, T.E., 2007. Statistical Parametric Mapping: The Analysis of Functional Brain Images. Academic Press London.

Persichetti, A.S., Avery, J.A., Huber, L., Merriam, E.P., Martin, A., et al., 2020. Layer-specific contributions to imagined and executed hand movements in human primary motor cortex. Curr. Biol. 30, 1–5. doi:10.2139/ssrn.3482808.

Pfeuffer, J., Adriany, G., Shmuel, A., Yacoub, E., Moortele, P.-f.V.D., Hu, X., Ugurbil, K., et al., 2002. Perfusion-based high-resolution functional imaging in the human brain at 7 Tesla. Magn. Reson. Med. 911, 903–911. doi:10.1002/mrm.10154.

Piechnik, S.K., Evans, J., Bary, L.H., Wise, R.G., Jezzard, P., et al., 2009. Functional changes in CSF volume estimated using measurement of water T2 relaxation. Magn. Reson. Med. 61 (3), 579–586. doi:10.1002/mrm.21897.

Polimeni, J.R., Uludağ, K., 2018. Neuroimaging with ultra-high field MRI: present and future. Neuroimage 168 (February), 1–6. doi:10.1016/j.neuroimage.2018.01.072.

Poplawsky, A.J., Fukuda, M., Murphy, M., Kim, S.G., et al., 2015. Layer-specific fMRI responses to excitatory and inhibitory neuronal activities in the olfactory bulb. J. Neurosci. 35 (46), 15263–15275. doi:10.1523/JNEUROSCI.1015-15.2015.

Poser, B.A., Norris, D.G., 2007. Measurement of activation-related changes in cerebral blood volume: VASO with single-shot HASTE acquisition. Magn. Reson. Mater. Phys., Biol. Med. 20 (2), 63–67. doi:10.1007/s10334-007-0068-0.

Poser, B.A., Setsompop, K., 2018. Pulse sequences and parallel imaging for high spatiotemporal resolution MRI at ultra-high field. Neuroimage 168 (December 2016), 101–118. doi:10.1016/j.neuroimage.2017.04.006.

Scheffler, K., Heule, R., Mario, G.B.-Y., Kardatzki, B., Lohmann, G., et al., 2018. The BOLD sensitivity of rapid steady-state sequences. Magn. Reson. Med. 81, 2526–2535. doi:10.1002/mrm.27585.

Schleicher, A., Palomero-Gallagher, N., Morosan, P., Eickhoff, S.B., Kowalski, T., De Vos, K., Amunts, K., Zilles, K., et al., 2005. Quantitative architectural analysis: a new approach to cortical mapping. Anat. Embryol. 210 (5–6), 373–386. doi:10.1007/s00429-005-0028-2.

Scouten, A., Constable, R.T., 2007. Applications and limitations of whole-brain MAGIC VASO functional imaging. Magn. Reson. Med. 58 (2), 306–315. doi:10.1002/mrm.21273.

Scouten, A., Constable, R.T., 2008. VASO-based calculations of CBV change: accounting for the dynamic CSF volume. Magn. Reson. Med. 59 (2), 308–315. doi:10.1002/mrm.21427.

Shen, Y., Kauppinen, R.A., Vidyasagar, R., Golay, X., et al., 2009. A functional magnetic resonance imaging technique based on nulling extravascular gray matter signal. J. Cereb. Blood Flow Metab. 29 (1), 144–156. doi:10.1038/jcbfm.2008.96.

Sicard, K., Shen, Q., Brevard, M.E., Sullivan, R., Ferris, C.F., King, J.A., Duong, T.Q., et al., 2003. Regional cerebral blood flow and BOLD responses in conscious and anesthetized rats under basal and hypercapnic conditions: implications for functional MRI studies. J. Cereb. Blood Flow Metab. 23 (4), 472–481. doi:10.1097/01.WCB.0000054755.93668.20.

Silva, A.C., Koretsky, A.P., 2002. Laminar specificity of functional MRI onset times during somatosensory stimulation in rat. Proc. Natl. Acad. Sci. 99 (23), 15182–15187. doi:10.1073/pnas.222561899.

Silva, A.C., Koretsky, A.P., Duyn, J.H., 2007. Functional MRI impulse response for BOLD and CBV contrast in rat somatosensory cortex. Magn. Reson. Med. 57 (6), 1110–1118. doi:10.1002/mrm.21246.

Smith, G.E., 1907. A new topographical survey of the human cerebral cortex, being an account of the distribution of the anatomically distinct cortical areas and their relationship to the cerebral sulci. J. Anat. Physiol. 41 (Pt 4), 237–254. http://www.ncbi.nlm.nih.gov/pubmed/17232738%0A http://www.pubmedcentral.nih.gov/articlerender.fcgi?artid=PMC1289123

Stelzer, J., Lohmann, G., Mueller, K., Buschmann, T., Turner, R., et al., 2014. Deficient approaches to human neuroimaging. Front. Hum. Neurosci. 8 (JULY), 1–16. doi:10.3389/fnhum.2014.00462.

Tian, P., Teng, I.C., May, L.D., Kurz, R., Lu, K., Scadeng, M., Hillman, E.M.C., De

Crespigny, A.J., D'Arceuil, H.E., Mandeville, J.B., Marota, J.J.A., Rosen, B.R., Liu, T.T., Boas, D.A., Buxton, R.B., Dale, A.M., Devor, A., et al., 2010. Cortical depth-specific microvascular dilation underlies laminar differences in blood oxygenation level-dependent functional MRI signal. Proc. Natl. Acad. Sci. 107 (34), 15246–15251. doi:10.1073/pnas.1006735107.

Trampel, R., Bazin, P. L., Pine, K., Weiskopf, N., et al., 2019. In-vivo magnetic resonance imaging (MRI) of laminae in the human cortex. Neuroimage 197, 707–715. doi:10.1016/j.neuroimage.2017.09.037.

Troprès, I., Grimault, S., Vaeth, A., Grillon, E., Julien, C., Payen, J.F., Lamalle, L., Décorps, M., et al., 2001. Vessel size imaging. Magn. Reson. Med. 45 (3), 397–408 doi:10.1002/1522-2594(200103)45:3%3C397::aid-mrm1052%3E3.0.co;2-3.

Truong, T.K., Song, A.W., 2009. Cortical depth dependence and implications on the neuronal specificity of the functional apparent diffusion coefficient contrast. Neuroimage 47 (1), 65–68. doi:10.1016/j.neuroimage.2009.04.045.

Turner, R., 2002. How much codex can a vein drain? Downstream dilution of activation-related cerebral blood oxygenation changes. Neuroimage 16 (4), 1062–1067. doi:10.1006/nimg.2002.1082.

Turner, R., 2013. Microstructural Parcellation of the Human Cerebral Cortex: From Brodmann's Post-Mortem Map to in Vivo Mapping with High-Field Magnetic Resonance Imaging. In: MRI Methods for In-Vivo Cortical Parcellation. Springer Berlin Heidelberg, pp. 197–220.

Uh, J., Lin, A.L., Lee, K., Liu, P., Fox, P., Lu, H., et al., 2011. Validation of VASO cerebral blood volume measurement with positron emission tomography. Magn. Reson. Med. 65 (3), 744–749. doi:10.1002/mrm.22667.

van Zijl, Hua, J., Lu, H., 2012. The BOLD post-stimulus undershoot, one of the most debated issues in fMRI. Neuroimage 62, 1092–1102. doi:10.1016/j.neuroimage.2012.01.029.

Vogt, C., Vogt, O., 1919. Allgemeinere ergebnisse unserer hirnforschung. J. Psychol. Neurol. 25, 279–461.

Vu, A.T., Gallant, J.L., 2015. Using a novel source-localized phase regressor technique for evaluation of the vascular contribution to semantic category area localization in BOLD fMRI. Front. Neurosci. 9 (NOV), 1–13. doi:10.3389/fnins.2015.00411.

Waehnert, M.D., Dinse, J., Weiss, M., Streicher, M.N., Waehnert, P., Geyer, S., Turner, R., Bazin, P.L., et al., 2014. Anatomically motivated modeling of cortical laminae. Neuroimage 93, 210–220. doi:10.1016/j.neuroimage.2013.03.078.

Wu, C.W., Liu, H.L., Chen, J.H., Yang, Y., et al., 2010. Effects of CBV, CBF, and blood-brain barrier permeability on accuracy of PASL and VASO measurement. Magn. Reson. Med. 63 (3), 601–608. doi:10.1002/mrm.22165.

Yablonskiy, D.A., Haacke, E.M., 1994. Theory of NMR signal behavior in magnetically inhomogeneous tissues: the static dephasing regime. Magn. Reson. Med. 32 (6), 749–763. doi:10.1002/mrm.1910320610.

Yacoub, E., Wald, L.L., et al., 2018. Pushing the spatio-temporal limits of MRI and fMRI. Neuroimage 164, 1–3. doi:10.1016/j.neuroimage.2017.11.034.

Yang, J., Yu, Y., 2019. Technological advances of ultra-high field laminar fMRI for study on layer-specific activation in the human brain. Med. Sci. Digest 45 (418), 418–421.

Yu, Y., Huber, L., Yang, J., Jangraw, D.C., Handwerker, D.A., Molfese, P.J., Chen, G., Ejima, Y., Wu, J., Bandettini, P.A., et al., 2019. Layer-specific activation of sensory input and predictive feedback in the human primary somatosensory cortex. Sci. Adv. 5 (5), eaav9053. doi:10.1126/sciadv.aav9053.

Zhao, F., Wang, P., Hendrich, K., Ugurbil, K., Kim, S.G., et al., 2006. Cortical layer-dependent BOLD and CBV responses measured by spin-echo and gradient-echo fMRI: insights into hemodynamic regulation. Neuroimage 30 (4), 1149–1160. doi:10.1016/j.neuroimage.2005.11.013.

Zong, X., Kim, T., Kim, S.G., 2012. Contributions of dynamic venous blood volume versus oxygenation level changes to BOLD fMRI. Neuroimage 60 (4), 2238–2246. doi:10.1016/j.neuroimage.2012.02.052.